

A simple stochastic quadrant model for the transport and deposition of particles in turbulent boundary layers

C. Jin,¹ I. Potts,¹ and M. W. Reeks^{1, a)}

*School of Mechanical & Systems Engineering, Newcastle University,
Stephenson Building, Claremont Road, Newcastle upon Tyne, NE1 7RU,
UK*

(Dated: 29 October 2018)

We present a simple stochastic quadrant model for calculating the transport and deposition of heavy particles in a fully developed turbulent boundary layer based on the statistics of wall-normal fluid velocity fluctuations obtained from a fully developed channel flow. Individual particles are tracked through the boundary layer via their interactions with a succession of random eddies found in each of the quadrants of the fluid Reynolds shear stress domain in a homogeneous Markov chain process. In this way we are able to account directly for the influence of ejection and sweeping events as others have done but without resorting to the use of adjustable parameters. Deposition rate predictions for a wide range of heavy particles predicted by the model compare well with benchmark experimental measurements. In addition deposition rates are compared with those obtained from continuous random walk (CRW) models and Langevin equation based ejection and sweep models which noticeably give significantly lower deposition rates. Various statistics related to the particle near wall behavior are also presented. Finally we consider the model limitations in using the model to calculate deposition in more complex flows where the near wall turbulence may be significantly different.

Keywords: Turbulent deposition, quadrant analysis, stochastic model, heavy particles, boundary layer

^{a)}Electronic mail: mike.reeks@ncl.ac.uk

I. INTRODUCTION

In this paper, we propose a simple stochastic quadrant model of coherent structures for heavy particle deposition in a turbulent boundary layer inspired by the quadrant analysis of Willmarth and Lu¹ which captures the influence of sweeps and ejections on the deposition of particles. It is another way of modeling deposition of heavy particles within fully developed turbulent boundary layers that adds insight and suggests new ways for improving the deposition prediction of heavy particles encountered in a wide range of industrial and environmental applications².

Our objective is to show how the influence of ejection and sweeping events in a turbulent boundary layer on particle deposition can be taken account of in a simple and more transparent way than in other models with no adjustable constants or parameters and at the same time preserving the statistics of the near wall turbulence. These are features of course that make the model highly suited for implementation in Reynolds-Averaged Navier-Stokes (RANS) CFD codes like FLUENT or Code_Saturne for the prediction of the deposition of heavy particles encountered in a wide range of industrial and environmental applications. However, it is the fundamental way this model deals with the sweeping and ejection events that is the focus of the study we report here.

The modelling and simulation of the transport and deposition of particles in a turbulent boundary layer have been and continue to be much studied topics. The first attempts of Friedlander and Johnstone³ and Davies⁴ were based on a gradient diffusion/free-flight theory where the concept of a particle stop distance was proposed. However the initial particle free-flight velocity had to be artificially adjusted from its value based on the local fluid rms velocity to get good agreement with the experimental data. Hutchinson, Hewitt, and Dukler⁵ and Kallio and Reeks⁶ employed a Monte-Carlo based Lagrangian particle tracking method for calculating particle deposition. In the work of Kallio and Reeks⁶ the turbulent boundary layer was described as a randomized eddy field with corresponding velocity and time scales as functions of the particle distance away from the wall. Swailes and Reeks⁷ proposed to use the kinetic equation developed by Reeks⁸ as a model to study the deposition of “high inertia” particles in a turbulent duct flow. Young and Leeming⁹ developed a simple approach based on an advection diffusion equation (ADE) to address the particle deposition in turbulent pipe flows, which represents a considerable advance

in physical understanding over previous free-flight theories. Guha¹⁰ developed a unified Eulerian theory, which is based on a Reynolds averaging of the particle continuity and momentum conservation equations for studying turbulent deposition onto smooth and rough surfaces. Zaichik *et al.*¹¹ developed a simplified Eulerian model called the diffusion-inertia model (DIM), which is based on a kinetic equation for the probability density function (PDF) of particle velocity and position, to investigate the dispersion and deposition of low-inertia particles in turbulent flows. Furthermore, the DIM was incorporated into the nuclear/industrial computational fluid dynamics (CFD) Code_Saturne for calculating the deposition of aerosols (see¹²).

More recently van Dijk and Swailes¹³ produced an extremely accurate numerical solution of a PDF equation which replicated exactly a random walk model simulation of particles in a turbulent boundary layer (similar to the statistical model used here but without explicitly involving the influence of the ejection and sweeps). This is an important step forward because observed features such as the concentration profiles, are not subject to statistical error or numerical inaccuracies and therefore are real effects as far as model predictions are concerned. So we can learn a great deal about the mechanisms of non-local inertial transport, albeit for a relatively simple random walk model, particularly the process of trapping of particles in boundary layers and the occurrence of a singularity in the particle concentration very close to the wall, which makes no contribution to the deposition.

Thanks to significant progress achieved in CFD, and in particular in the development of sophisticated turbulence models and numerical methods for unstructured grids for complex geometry, the CFD approach has been used to study the deposition of heavy particles in both simple and complex flows and geometries. This is usually carried out in an Eulerian-Lagrangian framework where individual particles are tracked through a random Eulerian flow field in which the mean flow, the timescales and rms of the velocity fluctuations are based on a solution of a closed set of Reynolds-Averaged Navier-Stokes (RANS) equations for the underlying carrier-phase flow field. To obtain statistically significant results it is necessary to carry out the calculation for a huge number of particles, each particle associated with a particular realization of the random flow field. This facility has been embedded into most CFD codes, although the stochastic nature of both the turbulence of the underlying flow and the dispersed particulate flow makes the problem of turbulent dispersed particulate flows more complex than its single-phase counterpart.

Yet prediction of turbulent particle depositions based on the general RANS modelling framework still has its shortcomings as demonstrated by numerous researchers^{14–23} when comparing predictions with the benchmark experimental measurements of Liu and Agarwal²⁴. A particular inadequacy is the isotropic assumption used in the standard $k - \epsilon$ turbulence model of a general RANS modelling framework to calculate fluctuating fluid velocities $u'_i = \sqrt{2k/3}$. Associated with this is the structure and timescale of the near wall turbulence that is a critically controlling factor for the deposition of particles. To address this inadequacy, Guingo and Minier²¹ developed a sophisticated one-dimensional continuous random walk (CRW) boundary layer model to model the fluid fluctuating velocity and the interaction of particles with the near wall coherent structures (e.g. sweeps and ejections) explicitly. A similar methodology to account for the interaction of particles with sweeps and ejections has been employed by Chibbaro and Minier²², who obtained satisfactory predictions of deposition rates with the standard $k - \epsilon$ model in a general CFD modelling framework. Both Guingo and Minier²¹ and Chibbaro and Minier²² demonstrated the significant role played by the near wall coherent structures on the transport and deposition of heavy particles within turbulent boundary layers.

Since Kline *et al.*²⁵ first reported the presence of well-organized spatially and temporally dependent motions in the near wall region (referred to as bursting) of a turbulent flow, the role played by coherent structures of near wall on the transport and deposition of inertia particle has been the focus of attention of a number of researchers. Owen²⁶ was the first to suggest that the transport of fine solid particles from a turbulent gas stream to an adjoining surface may arise from sporadic violent eruptions from the viscous sublayer. Cleaver and Yates²⁷ proposed a sub-layer model, which takes into account the role of the up-sweeps and down-sweeps of fluid observed in the near wall region of turbulent flows, in order to obtain a better understanding of the mechanics of the particle deposition process. The model predictions were in satisfactory agreement with experimental measurements on deposition rates. The sub-layer model of Cleaver and Yates²⁷ was used by Fichman, Gutfinger, and Pnueli²⁸ and Fan and Ahmadi²⁹ for calculating particle deposition. Wei and Willmarth³⁰ carried out a quadrant analysis of laser Dropper anemometer (LDA) measurements of near wall fluid velocity in order to acquire a preliminary understanding of suspended sediment transport. Kaftori, Hetsroni, and Banerjee³¹ and Kaftori, Hetsroni, and Banerjee³² demonstrated the importance of coherent wall structures on particle motion in a turbulent boundary layer and

on subsequent entrainment and deposition processes via a series of systematic experiments. Marchioli and Soldati³³ further examined the mechanisms for particle transfer and segregation in turbulent boundary layers through Direct Numerical Simulation (DNS) calculations of channel flow. They revealed that downward sweeps, referred to as quadrant IV events, cause particles to transfer to the near wall region where particles preferentially accumulate in the low-speed streaks, whilst ejections, referred to as quadrant II events bring about the migration of particles to the region of outer flow. Soldati and Marchioli³⁴ provided a systematic review and physical insight into the physics and modelling of deposition and entrainment of particles from turbulent flows which has been a catalyst for better models of particle deposition.

The work of Wei and Willmarth³⁰ has been particularly important in developing and implementing the methodology for calculating the particle transport in a turbulent boundary layer proposed in this paper. They performed the quadrant analysis of Willmarth and Lu¹ to examine the high-resolution, two-component laser-Doppler anemometer measurements of the wall normal fluid velocity fluctuations in a fully developed water channel flow. They found that there is a net upward momentum flux in the range of $y^+ > 30$ that may be associated with the bursting process occurring in quadrant II, whilst there is a net downward momentum flux in the range of $10 \leq y^+ \leq 30$ that may be associated with the sweeps process occurring in quadrant IV. The net momentum flux results from the positively skewed distribution of the fluctuating wall-normal velocity. Inspired by this approach, the present work proposes another way to model near wall coherent structures and their interaction with particles under a positively skewed distribution of wall-normal fluctuating velocities.

It is worth noting that stochastic models of the type considered here are used to predict particle deposition in complex flows using commercial CFD codes like FLUENT or the open source Code_Saturne where they are used in conjunction with a RANS calculation for the underlying carrier flow. The near wall flow is based on the application of suitable wall functions which assume a log-law region and the scaling of the mean flow and turbulence on a local shear stress (friction velocity) which is part of the solution of the RANS calculation. The profiles of the mean flow and the turbulence are thus appropriate for a fully developed turbulent boundary layer. In incorporating our model here into a RANS calculation of the carrier flow we would be making the same assumption about the statistics we employ. It is of course perfectly compatible with the type of wall function that is being employed but

the assumption of similarity to that of a fully developed turbulent boundary is a major assumption that needs to be tested.

In formulating and examining this approach, this paper is structured as follows. First, the stochastic quadrant model is formulated and discussed. We then present the statistics in the four quadrants obtained using a quadrant analysis of the wall-normal fluid velocity fluctuations acquired from an LES of a fully developed channel flow. Finally, results for the deposition rates from an implementation of this stochastic quadrant model are presented and compared with results from benchmark experimental measurements, and those obtained from a one-dimensional Langevin equation-based CRW model and other CRW models. Several statistics concerning the transported particles in the near wall region are also shown.

II. MODELLING METHODOLOGY

A. Governing equations of particle motion

A Lagrangian particle tracking module was developed and coupled with an unstructured cell-centred finite-volume based Navier-Stokes equation solver to calculate trajectories of heavy particles in flow fields. The focus of this work is on the deposition of non-colliding, rigid, spherical and heavy particles. For the numerical simulations presented here the ratio of particle density (920 kg/m³) to fluid density is 770, which is the same as the experimental measurements of Liu and Agarwal²⁴. Density ratio is particular to the calculations presented, and not a fundamental part of model. The concentration of particles is dilute enough to assume one-way coupling. The particle equation of motion discussed by Maxey and Riley³⁵ is simplified in this work by taking into account only the drag force. We thus can write the particle equation of motion involving the non-linear form of the drag law with the point particle approximation

$$\frac{d\mathbf{v}_p}{dt} = \frac{1}{\tau_p} C_D \frac{Re_p}{24} (\mathbf{u} - \mathbf{v}_p), \quad (1)$$

where \mathbf{v}_p is the particle velocity and \mathbf{u} the instantaneous fluid velocity at the particle position for a particle with response time τ_p . Previous research effort on particle dispersion in a turbulent channel flow (see³⁶) has demonstrated that the particle Reynolds number, $Re_p = |\mathbf{u} - \mathbf{v}_p|d_p/\nu$ does not necessarily remain small enough to assume Stokes drag. Thus, an empirical relation for C_D from Morsi and Alexander³⁷, which is applicable to a wide range

of particle Reynolds number with sufficiently high accuracy, is employed, namely

$$C_D = c_1 + \frac{c_2}{Re_p} + \frac{c_3}{Re_p^2}, \quad (2)$$

in which c_1, c_2, c_3 are constants and provided by Morsi and Alexander³⁷. The above empirical expression exhibits the correct asymptotic behavior at low as well as high values of Re_p ³⁸.

The position \mathbf{x}_p of particles is obtained from the kinematic relationship

$$\frac{d\mathbf{x}_p}{dt} = \mathbf{v}_p. \quad (3)$$

The boundary condition for the above equation is that the particle is captured by the wall when its center is less than its radius away from the nearest wall. It is worth pointing out here that the present stochastic quadrant model does not take into account the effect of build-up of deposited particles on the incoming particles. The particle capture is assumed to be perfectly absorbing with no subsequent re-suspension.

From a converged RANS computation of the velocity flow field, Eq: (3) is integrated in time using the second-order Adams-Bashforth scheme to obtain particle trajectories, whilst Eq: (1) is integrated with the second-order accurate Gear2 (backward differentiation formulae) scheme to obtain instantaneous velocity of particles. Fluid velocities solved are stored at the centroids of grid cells on the basis of using cell-centred finite-volume scheme. Since it is only by chance that a particle coincides with the cell centroid, a quadratic scheme based on velocity gradient reconstruction is used to interpolate the fluid velocity to the particle location. The collective statistical properties of the particle phase are obtained by following the trajectories of 10^5 particles.

B. Formulation of the stochastic quadrant model

The discrete random walk (DRW, also known as Monte-Carlo eddy interaction) model is the basis of the formulation of the present stochastic model. The fluid velocity field in the absence of the dispersed particle phase is determined by a RANS computation with the standard $k-\epsilon$ model (see³⁹). The temporal fluctuations of the velocity field are described by a sequence of discrete eddies, with which the suspended particles interact for a randomized eddy lifetime. In the particle equation of motion (1), the instantaneous fluid velocity is represented by a Reynolds decomposition of averaged and fluctuating components, $\mathbf{u} = \bar{\mathbf{U}} +$

\mathbf{u}' . The time-averaged fluid velocity $\bar{\mathbf{U}}$ is acquired from the solution of a RANS calculation for the turbulent flow. Thus it is crucial to model the fluctuating components to account for the effect of turbulence on the dispersion of particles. In this respect, there have been a number of attempts that we have referred to in the introduction (see also^{17,18,20-23}).

In this work, our attention is confined to the turbulent deposition of particles onto perfectly absorbing adjacent surfaces in a fully developed turbulent boundary layer, in which the flow velocity statistics are independent of the streamwise coordinate x . As stated by Pope⁴⁰, a fully developed channel flow can be considered as statistically stationary and one-dimensional, with velocity statistics depending only on the wall normal direction y . In this case, a new approach is proposed here to model the wall-normal fluctuating velocity component denoted by v' based on quadrant analysis of the coupled (u', v') Reynolds shear stress domain. In addition, particle tracking is performed using the Lagrangian approach.

It is widely considered that the distribution of the wall normal fluctuating velocity is skewed within fully developed turbulent boundary layers (see⁴¹). The wall normal fluctuating velocity component v' can be distinguished as positive or negative according to whether the momentum flux is away from or towards the wall. Thus let v'_+ be a function defined as

$$v'_+ = \begin{cases} v' & \text{if } v' > 0, \\ 0 & \text{if } v' \leq 0 \end{cases} \quad (4)$$

and v'_- defined as

$$v'_- = \begin{cases} v' & \text{if } v' < 0, \\ 0 & \text{if } v' \geq 0. \end{cases} \quad (5)$$

It is possible to define the average value of v'_+ and v'_- as: $\langle v'_+ \rangle = \frac{1}{T_+} \int_0^T v'_+ dt$ and $\langle v'_- \rangle = \frac{1}{T_-} \int_0^T v'_- dt$, where T is the interval of observation time containing the fraction of v'_+ denoted by T_+ and the fraction of v'_- denoted by T_- . We then have $\langle v'_+ \rangle + \langle v'_- \rangle = \frac{1}{T_+} \int_0^T \left(v'_+ + \frac{T_+}{T_-} v'_- \right) dt$. Accordingly,

$$\frac{1}{T} \int_0^T (v'_+ + v'_-) dt = 0. \quad (6)$$

Thus if $T_+ < T_-$,

$$|\langle v'_+ \rangle| > |\langle v'_- \rangle|, \quad (7)$$

if $T_+ > T_-$,

$$|\langle v'_+ \rangle| < |\langle v'_- \rangle|. \quad (8)$$

Similarly, average momentum flux per unit area can be defined as:

$$\langle v'^2_+ \rangle = \frac{1}{T_+} \int_0^{T_+} (v'_+)^2 dt \quad (9)$$

and

$$\langle v'^2_- \rangle = \frac{1}{T_-} \int_0^{T_-} (v'_-)^2 dt. \quad (10)$$

According to Eq: (7), when $T_+ < T_-$ we have

$$|\langle v'^2_+ \rangle| > |\langle v'^2_- \rangle|, \quad (11)$$

and according to Eq: (8), when $T_+ > T_-$

$$|\langle v'^2_+ \rangle| < |\langle v'^2_- \rangle|. \quad (12)$$

It is obvious that $|\langle v'^3_+ \rangle| > |\langle v'^3_- \rangle|$ when $T_+ < T_-$; whilst $|\langle v'^3_+ \rangle| < |\langle v'^3_- \rangle|$ when $T_+ > T_-$. These two cases mean that the wall normal fluctuating component is derived from positively and negatively skewed distributions, respectively. Under the positively skewed distribution, there will be a net upward momentum flux of fluid; whilst under the negatively skewed distribution, there will be a net downward momentum flux of fluid. This imbalance of momentum flux of fluid particle within fully turbulent boundary layers can play an important role on the transport and deposition of heavy particles. The data from Kim, Moin, and Moser⁴¹ show that the wall normal fluctuating component is of positive skewness in the range of $0 < y^+ < 10$ and $y^+ > 30$ and of negative skewness in the range of $10 < y^+ < 30$.

C. Statistics of v' in each of the four quadrants

Following the quadrant analysis approach of Willmarth and Lu¹ for analysing the structure of the Reynolds stresses, we classified the wall normal fluctuating velocity and averaged it in the four quadrants according to the instantaneous flow velocity in the quadrant domain. In this sense, the instantaneous velocity of a sufficiently large number of fluid particles at a

specified position may be categorized in terms of the sign of the streamwise and wall normal velocity fluctuations. For example, when both u' and $v' > 0$ the instantaneous velocity signal is allocated to quadrant I (Q_I); in the case of $u' < 0$ and $v' > 0$, it is allocated in quadrant II (Q_{II}); when both u' and $v' < 0$, is allocated to the quadrant III (Q_{III}); finally, if $u' > 0$ and $v' < 0$, it is allocated to quadrant IV (Q_{IV}). We note that upward momentum fluxes may be associated primarily with the bursting process associated with events in Q_{II} , whilst downward momentum fluxes are associated with sweep events in Q_{IV} . Physically speaking, upward momentum fluxes associated with Q_{II} would cause particles to move away from the wall and downward momentum fluxes associated with Q_{IV} would result in the migration of particles toward the wall.

Time averages of v'_i and momentum flux $v_i'^2$ can be defined for each of the four quadrants according to Eq: 7 and 9 as

$$\langle v'_i \rangle = \frac{1}{T_i} \int_0^T v'_i dt; \quad i = I, II, III, IV \quad (13)$$

and

$$\langle v_i'^2 \rangle = \frac{1}{T_i} \int_0^T v_i'^2 dt; \quad i = I, II, III, IV, \quad (14)$$

where T_i denotes time spell spent in the quadrant i by v'_i , and v'_i is define as

$$v'_i = \begin{cases} v' & \text{if } v' \text{ satisfies the criterion of quadrant analysis,} \\ 0 & \text{if not.} \end{cases} \quad (15)$$

A large eddy simulation (LES) of a fully developed channel flow with $Re_\tau = 180$ was carried out to obtain the corresponding statistics of v'_i up to $y^+ = 100$. The LES was based on a dynamic Smagorinsky sub-grid scale (SGS) model⁴² and a generalized fractional-step method⁴³ for the overall time-advancement. A scatter plot of u' and v' together with the corresponding probability density function (pdf) (statistically integrated over a non-dimensional time unit) is shown in FIG. 1 according to the quadrant analysis¹. We find that the probability density functions of u' and v' are both skewed.

In FIG. 2, the quadrant mean $\langle v'_i \rangle$ and wall normal flow velocity rms $\langle v_i'^2 \rangle^{1/2}$ as a function of y^+ show that the fluctuating components in the four quadrants are smaller in magnitude than the wall normal flow velocity rms $\langle v_i'^2 \rangle^{1/2}$ across the y^+ range shown. $\langle v'_i \rangle$ in each of the four quadrants is of different magnitude, indicating that there is an asymmetry in the wall normal fluctuating components. Furthermore, the greatest magnitude of $\langle v'_i \rangle$ is found

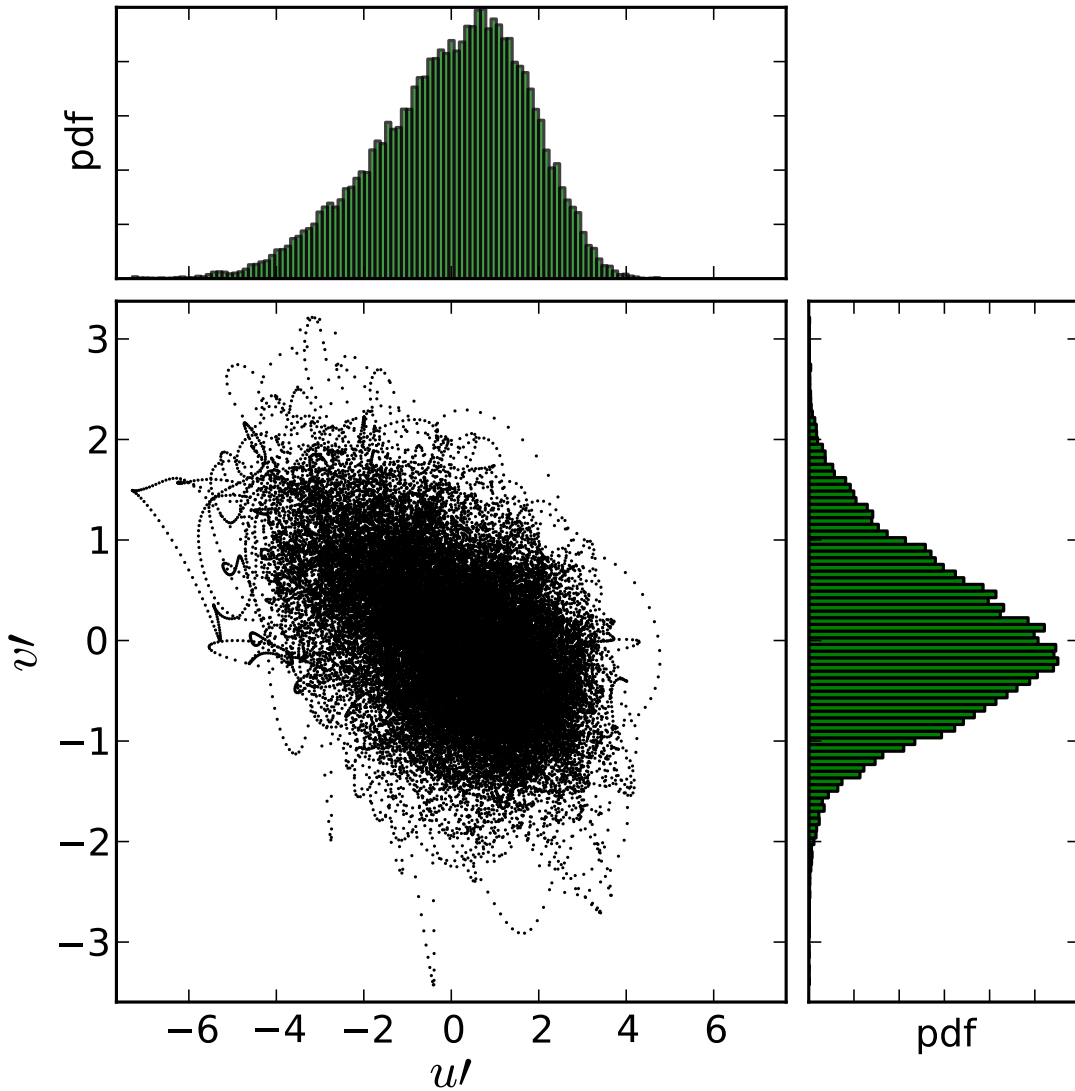


FIG. 1: Scatter plot of u' and v' at $y^+ = 50$ resolved by LES, categorised in terms of quadrant analysis.

in Q_{II} across most of the y^+ range. FIG. 3 shows that there is a net upward momentum flux resulting from Q_{II} for the range of $y^+ > 20$. However, this situation is reversed in the range of $y^+ < 20$. The asymmetry of $\langle v'_i \rangle$ and $\langle v_i'^2 \rangle$ in each of the four quadrants is a new feature for modelling velocity fluctuations encountered by heavy particles, which we believe is particularly useful for measuring particle transport and deposition in the near wall region.

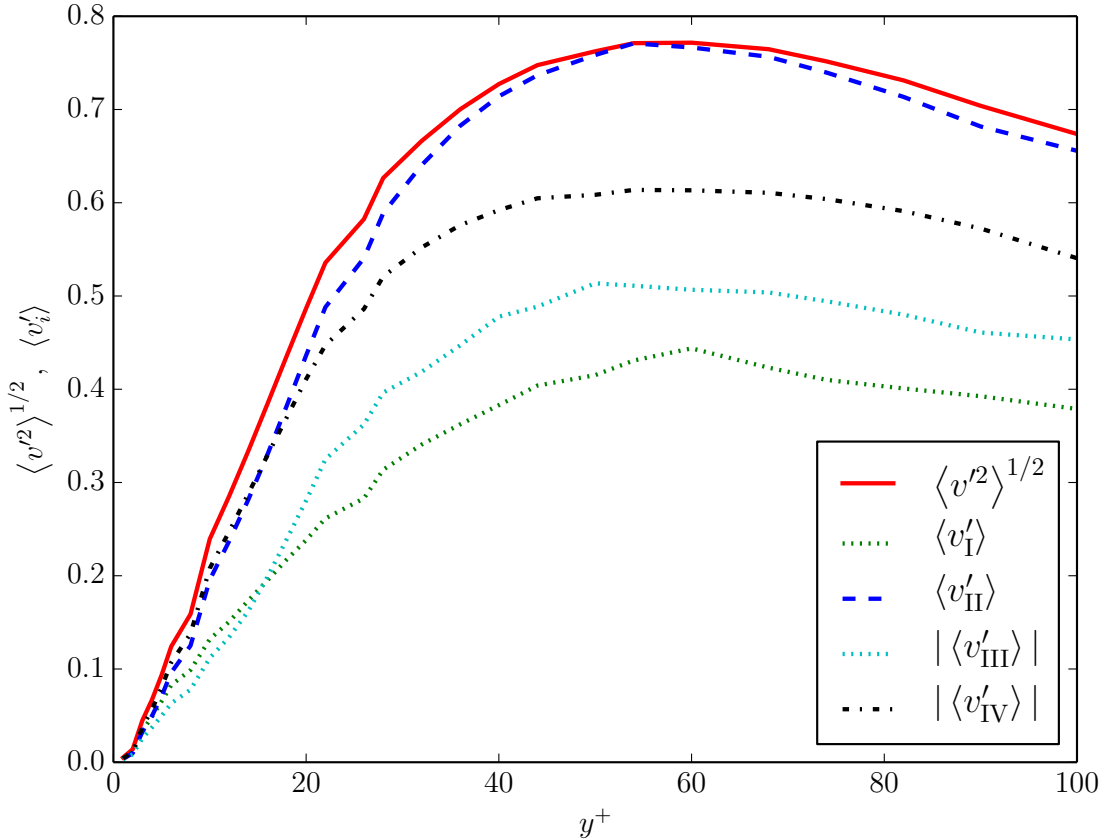


FIG. 2: Profiles of $\langle v'^2 \rangle^{1/2}$ and $\langle v'_i \rangle$ as a function of y^+ at $Re_\tau = 180$ in each of the four quadrants.

D. Implementation of the stochastic quadrant model

The imbalance of $\langle v'_i \rangle$ within each of the four quadrants will be of differing importance to the transport and deposition of heavy particles. Events in quadrant II are mainly associated with violent ejections of low-speed fluid away from the wall; motions in quadrant IV are primarily associated with an inrush of high-speed fluid toward the wall, also referred to as the sweeping event. There are no significant structures associated with quadrant I and III. The upward momentum flux in quadrant II may be a strongly contributing factor in the transport of particles away from the wall, reducing the deposition rates; whilst the inward momentum flux in quadrant IV may be a strongly contributing factor in the transport of particles towards the wall, tending increase the deposition rates.

The results on $\langle v'_i \rangle$ and $\langle v_i'^2 \rangle$ enables us to specify the statistics of wall-normal velocity

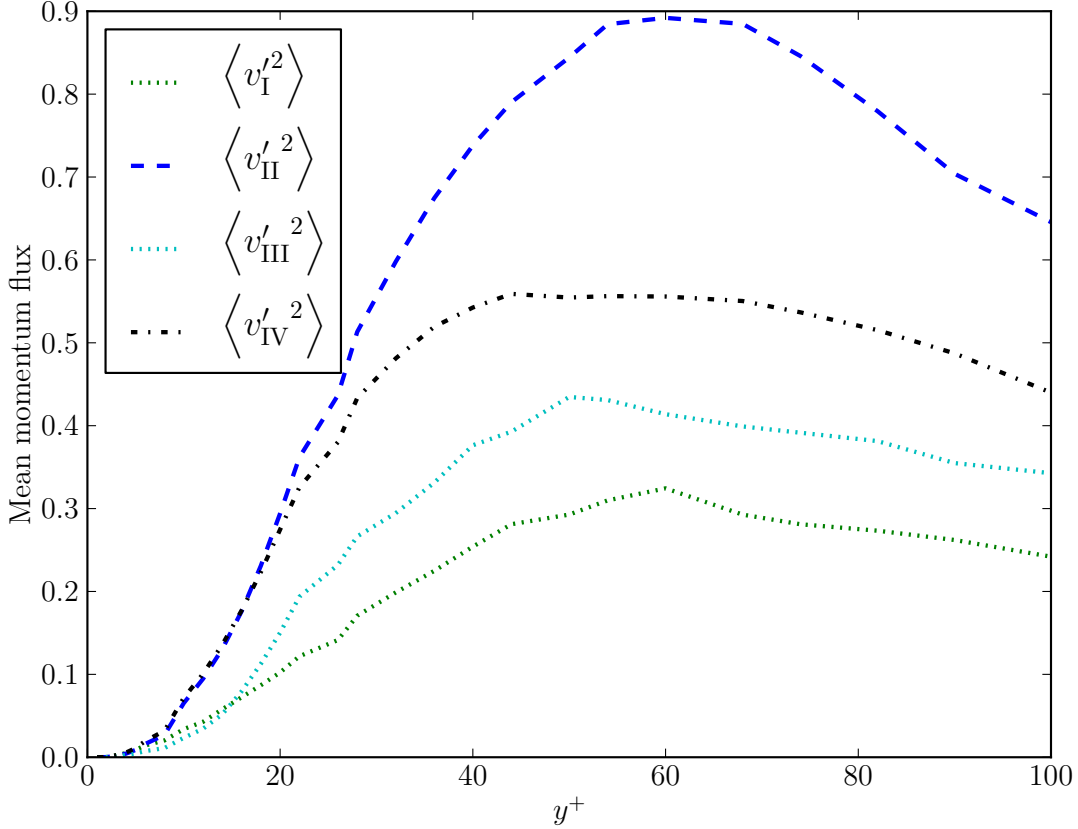


FIG. 3: Profiles of momentum fluxes as a function of y^+ at $Re_\tau = 180$ in each of the four quadrants.

fluctuations encountered by particles in each eddy along their trajectories. For example, curve-fitting of the four profiles of $\langle v'_i \rangle$ can be achieved easily. However, comparing the shape of $\langle v'_i \rangle$ with the shape of $\langle v'^2 \rangle^{1/2}$, a different scale factor is assumed between $\langle v'_i \rangle$ and $\langle v'^2 \rangle^{1/2}$. In FIG. 4 the probability density functions for a half normal distribution for v'_i in each of the four quadrants at $y^+ = 30$ are shown to be in fair agreement with the original LES results, indicating that a half normal distribution may be used to describe the distribution of v'_i . This probability distribution function is given by

$$f_\Omega(\omega; \sigma) = \begin{cases} \frac{\sqrt{2}}{\sigma\sqrt{\pi}} \exp\left(-\frac{\omega^2}{2\sigma^2}\right) & \text{if } \omega \geq 0, \\ 0 & \text{if } \omega < 0, \end{cases} \quad (16)$$

where σ is set to equal to the value of $\sqrt{\frac{\pi}{2}} \langle v_i'^2 \rangle^{1/2}$ at the corresponding y^+ location.

The logical next step is to construct a random process, which models the eddy motions in

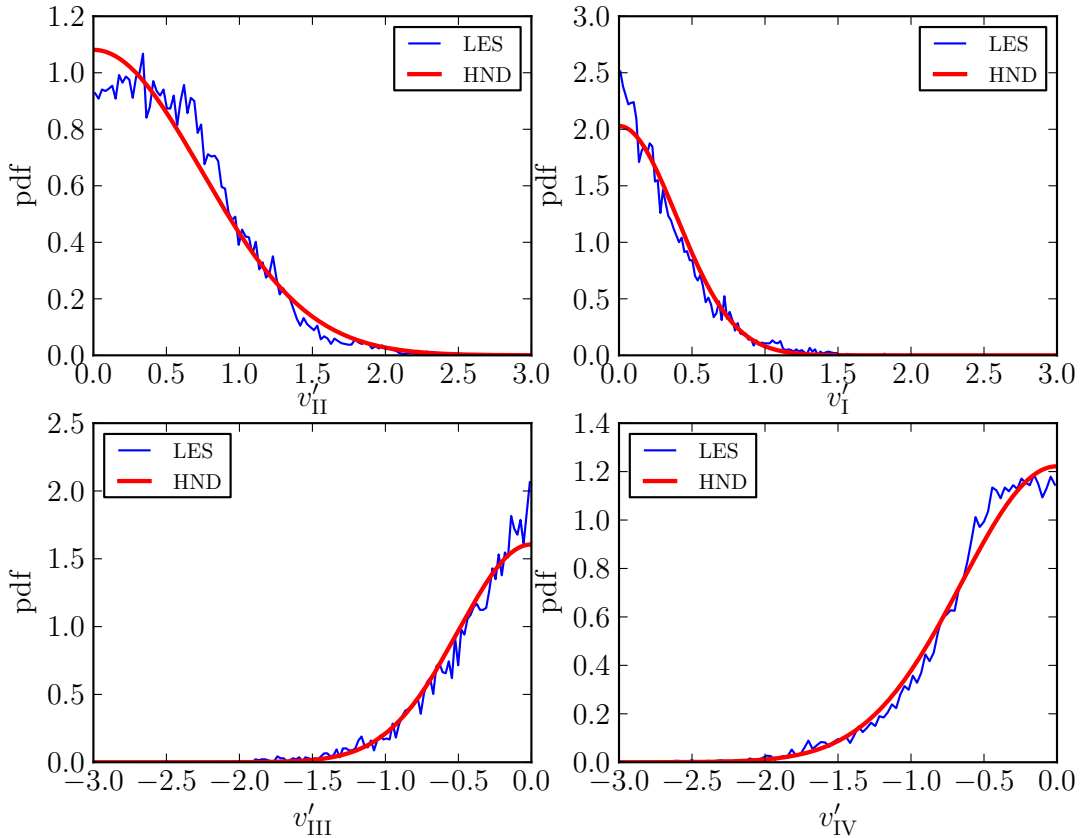


FIG. 4: Probability density function (pdf) for v'_i obtained by LES and a comparison with a half normal distribution (HND)

the four quadrants. Particles will interact with a random succession of eddies resulting from different quadrants. For this, a homogeneous Markov chain was conceived as a model for the evolution of eddy events in the four quadrants along the particle trajectories. Particles may interact with an eddy in quadrant I. After this eddy decays, they would then be able to interact with an eddy resulting from any of the four quadrants with a certain transition probability. FIG. 5 describes this process.

As far as the transition probabilities are concerned, let $Q_i, i = \{I, II, III, IV\}$ be a discrete time Markov chain on $\{Q_I, Q_{II}, Q_{III}, Q_{IV}\}$ with a transition matrix

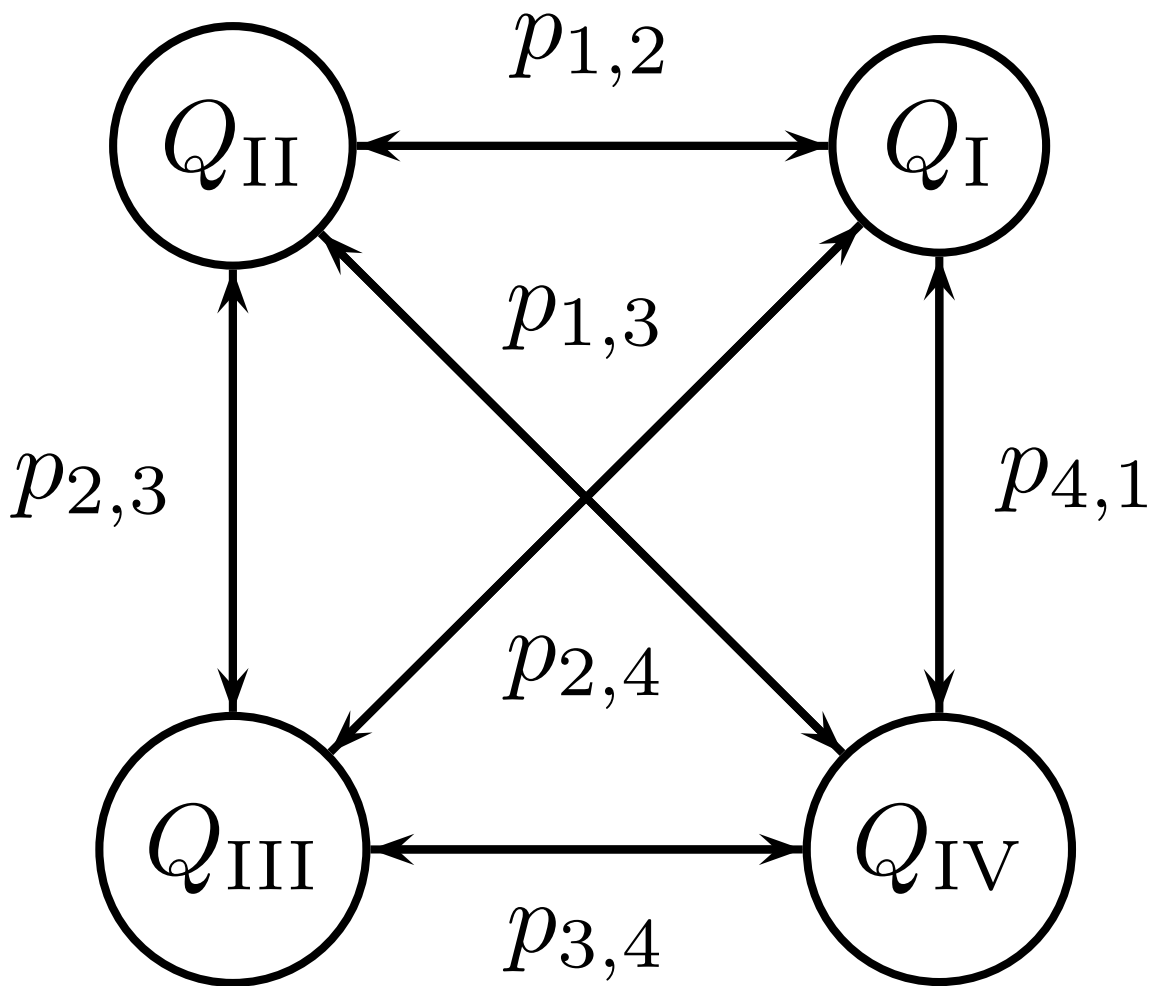


FIG. 5: Diagram describing the Markov chain modelling motions in the four quadrants.

$$P = \begin{pmatrix} p_{11} & p_{12} & p_{13} & p_{14} \\ p_{21} & p_{22} & p_{23} & p_{24} \\ p_{31} & p_{32} & p_{33} & p_{34} \\ p_{41} & p_{42} & p_{43} & p_{44} \end{pmatrix}, \quad (17)$$

where $(p_{ij} : i, j \in \{1, 2, 3, 4\})$ denotes the corresponding probability distribution of random eddy events in each quadrant. The transition matrix in Eq: 17, needs to satisfy the condition $\sum_j p_{ij} = 1$. For eddy events in the four quadrants, Eq: 17 is reduced to a “degen-

erate" transition matrix as

$$P = \begin{pmatrix} p_{11} & p_{22} & p_{33} & p_{44} \end{pmatrix}. \quad (18)$$

FIG. 6 shows variations of the relative probability associated with each of the four quadrants as a function of y^+ , which are computed in terms of the sign of each individual event within the integrated non-dimensional time. These probabilities are used as the transition probabilities denoted in Eq: (18).

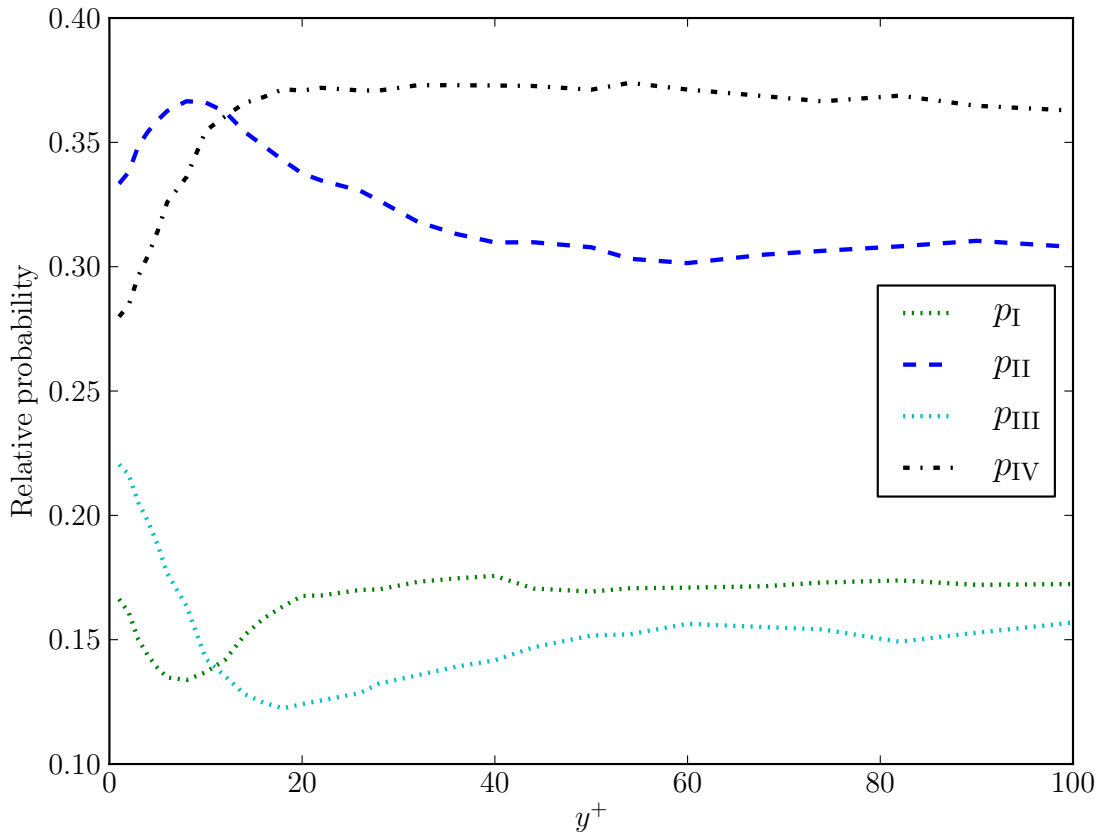


FIG. 6: Relative probability of four quadrants as a function of y^+ .

The time scale of eddies in each of the four quadrants is difficult to estimate accurately from the present study, although Luchik and Tiederman⁴⁴ provided several quantitative techniques to measure time scales associated with bursting events. In the present study, the lifetime of eddies in the four quadrants are assumed to equal to the Lagrangian time scale of fluid particles according to their corresponding y^+ position. FIG. 7 shows the Lagrangian time scale of fluid particles within turbulent boundary layers. This is taken from the curve-

fitting of Kallio and Reeks⁶. Furthermore, the random Lagrangian time scale ξ is assumed to obey an exponential distribution with the following PDF

$$f(\xi, T_L) = \frac{1}{T_L} e^{-\frac{\xi}{T_L}} \quad \xi > 0, \quad (19)$$

where T_L indicates the integral Lagrangian time scale in wall units at the particle position. FIG. 7 also shows the wall-normal rms profile of fluid velocity. $\langle v'_i \rangle$ in each of the four quadrants is obtained by multiplying $\langle v'^2 \rangle^{1/2}$ by a scaling factor that is the ratio of the magnitude of the velocity fluctuation in each of the four quadrants to the magnitude of wall-normal velocity fluctuation across the boundary layer. In every eddy generated in the four quadrants, the fluctuating velocity is sampled from a half normal distribution with a mean $\langle v'_i \rangle$ and a variance corresponding to the particular particle y^+ value in the boundary layer.

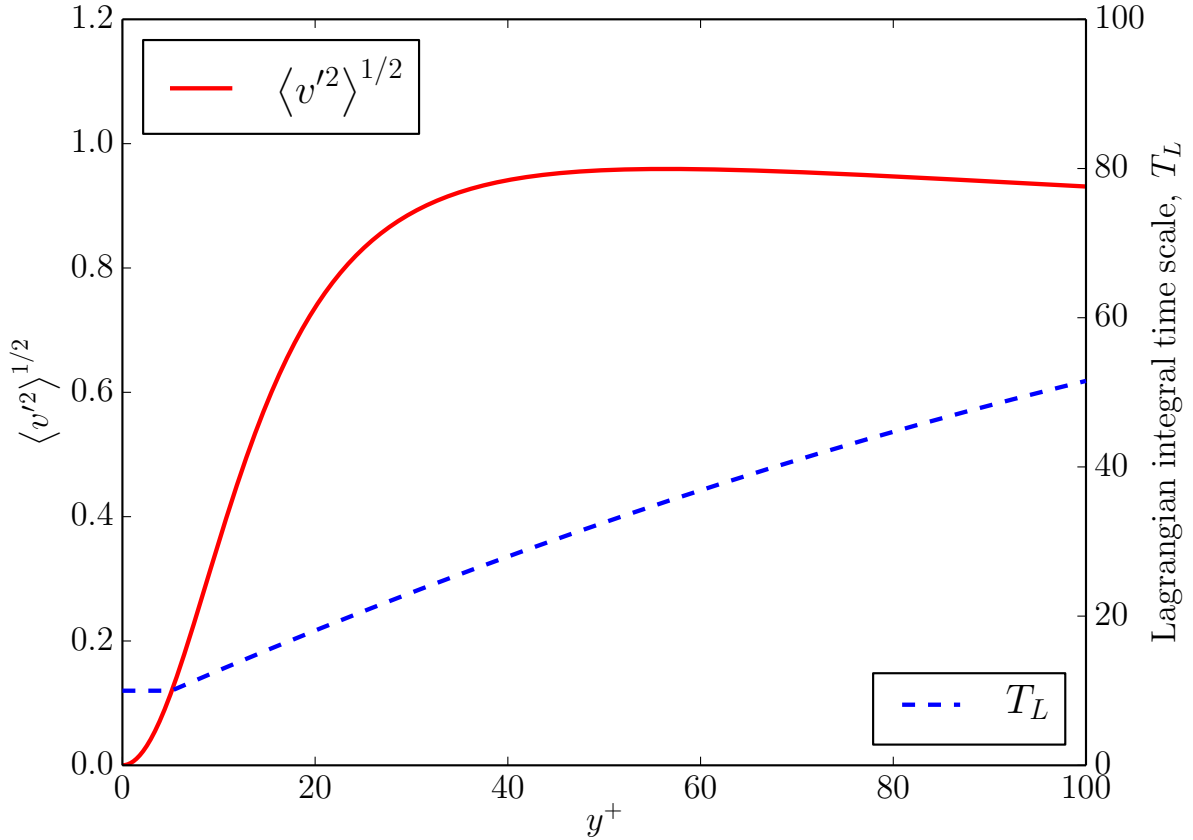


FIG. 7: Non-dimensional wall normal fluid velocity and Lagrangian time integral time scale as a function of y^+ within turbulent boundary layers.

The present stochastic model used to predict the deposition rates of inertial particles can be summarized in terms of the following steps: firstly, a RANS simulation is run to establish a steady flow field; secondly, velocity fluctuations encountered along the particle trajectories are generated within the discrete Markov chain Monte-Carlo process according to the relevant statistics; thirdly, Eqs: 1 and 3 are integrated to determine the particle trajectories; finally, the deposition rate can be calculated according to the penetration efficiency.

III. RESULTS AND DISCUSSION

A. Continuous phase

The turbulent boundary layer was resolved using the standard $k - \epsilon$ model with enhanced wall treatment. The y^+ value of the first cell adjacent to the wall was set at $y^+ = 1$. Two points need to be made here. Firstly, there is no discernible discrepancy between the inlet and middle plane velocity profiles. Secondly, although the calculated wall-friction velocity normalized velocity profiles show under-predicted values when compared with the DNS data of Kim, Moin, and Moser⁴¹, they show a very good agreement with the DNS data of Kim, Moin, and Moser⁴¹ when $y^+ < 10$. Given the fact that RANS was employed, the small difference between the calculated and DNS values shown in FIG. 8 for $y^+ > 10$ is reasonable. To avoid a transition region near the inlet region, an established velocity profile was injected as velocity boundary condition on the the inlet plane.

B. Dispersed particle phase

1. Particle deposition rates

The particle deposition rate in a turbulent boundary layer is usually quantified through a mass transfer coefficient K defined as

$$K = \frac{J_w}{\bar{c}}, \quad (20)$$

where J_w represents the particle flux onto the wall per unit area and time and \bar{c} is the average particle concentration within the boundary layer. The computation technique proposed by Kallio and Reeks⁶ was used to calculate the non-dimensional particle deposition velocity

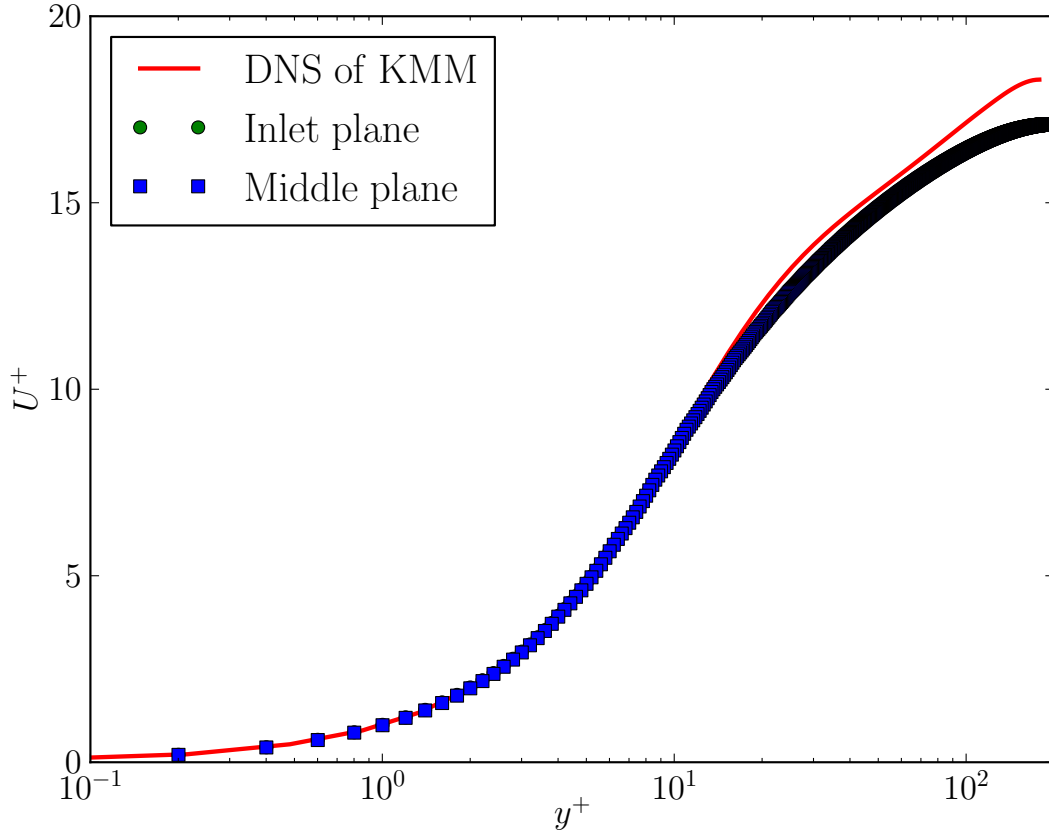


FIG. 8: Mean fluid velocity profiles from the inlet and middle plane.

defined as

$$V_{dep}^+ = \frac{\bar{U}A}{u_\tau P \Delta x} \ln \left(\frac{N_{in}}{N_{out}} \right) \quad (21)$$

where \bar{U} is the average streamwise fluid velocity across the fully developed turbulent boundary layer, A is the boundary layer cross sectional area, P the duct perimeter, Δx is the incremental length of section considered, and N_{in} and N_{out} are the total number of particles passing through the start and end plane of each section, respectively. The characteristic wall friction velocity u_τ was used to obtain the non-dimensional deposition velocity V_{dep}^+ . On the basis of Eq: 21, it can be inferred that the non-dimensional particle deposition velocity from the calculated fluid mean velocity profiles shown in FIG. 8 will be under-predicted when compared with the theoretical values. However, given the small difference shown in FIG. 8, the under-prediction will not significantly affect the final accuracy of the calculation of the non-dimensional particle deposition velocity. In this study, 10^5 particles are introduced uni-

formly from the inlet plane and their velocities are initialized to the value of the local fluid mean velocity.

Computed dimensionless particle deposition velocities are compared with the benchmark experimental measurements (see²⁴), the empirical curve-fit of McCoy and Hanratty⁴⁵ and the deposition velocities predicted by the standard $k - \epsilon$ model in FIG. 9. We have also included for comparison the results from Guingo and Minier²¹, who developed a sophisticated stochastic model to account for the geometrical structures in turbulent boundary layers and which like the current model accounts for the influence of sweeping and ejection events. It can be observed that very good agreement exists between the present computed results and experimental data in the range of $St > 5$. For $St < 5$, the stochastic quadrant model gives an under-prediction of the deposition rates. These are also features of the stochastic model of Guingo and Minier²¹ (G&M) which predicts significantly less deposition than obtained in this study throughout the entire range of St .

In addressing the reasons for the lack of agreement between the predictions of the present model and that of the G&M sweep and ejection model, it is worth considering some of the critical assumptions that were made by G&M in the formulation of their model. Referring to FIGs. 15 and 16 of Guingo and Minier²¹, we note that the turbulent boundary layer is divided into outer and inner zones: in the outer zone a fluid point is transported by a random succession of coherent structures which model the influence of ejections and sweeps together with phases in which the flow velocity field is more random and less persistent and described by a simple Langevin diffusion process; in the inner zone closest to the wall there are no coherent structures and the fluid point motion is driven by diffusion. What is important is that introducing 1D coherent structures into the outer zone should be consistent with the measured statistics of the turbulent boundary layer. FIG. 15 of Guingo and Minier²¹ shows the comparison of the G&M model predictions of the turbulent kinetic energy k and those obtained from DNS. There is a noticeable difference in the near wall region where the G&M profile of k is significantly steeper. The authors indicate that the profile of k depends markedly on the position of the interface between the outer and inner zones (as one might expect). In their simulation y_{int} , which is the interface distance away from the wall, varies randomly between 5 and 20 wall units. Better agreement with DNS measurements for k are obtained if $5 < y_{int} < 40$ (see FIG. 16 of Guingo and Minier²¹). However in this case the predicted deposition rates are significantly worse (as one might expect since the curve is less

steep). Despite the fact that the k profile is noticeably different from that obtained using DNS, G&M stick with their initial choice for y_{int} because it gives better deposition results and consistent with their original assumption of the location of the sweeping and ejection events. The steeper profile of k compared with the DNS measurements may be regarded as an inevitable artifact and penalty one pays for using a simple model of 1D coherent structures. The model we have presented here contains the influence of ejection and sweeps reflected in the skewness of the measured DNS statistics and as such does not introduce spurious features into the deposition mechanisms. Therefore it is not subject to fine tuning of model parameters.

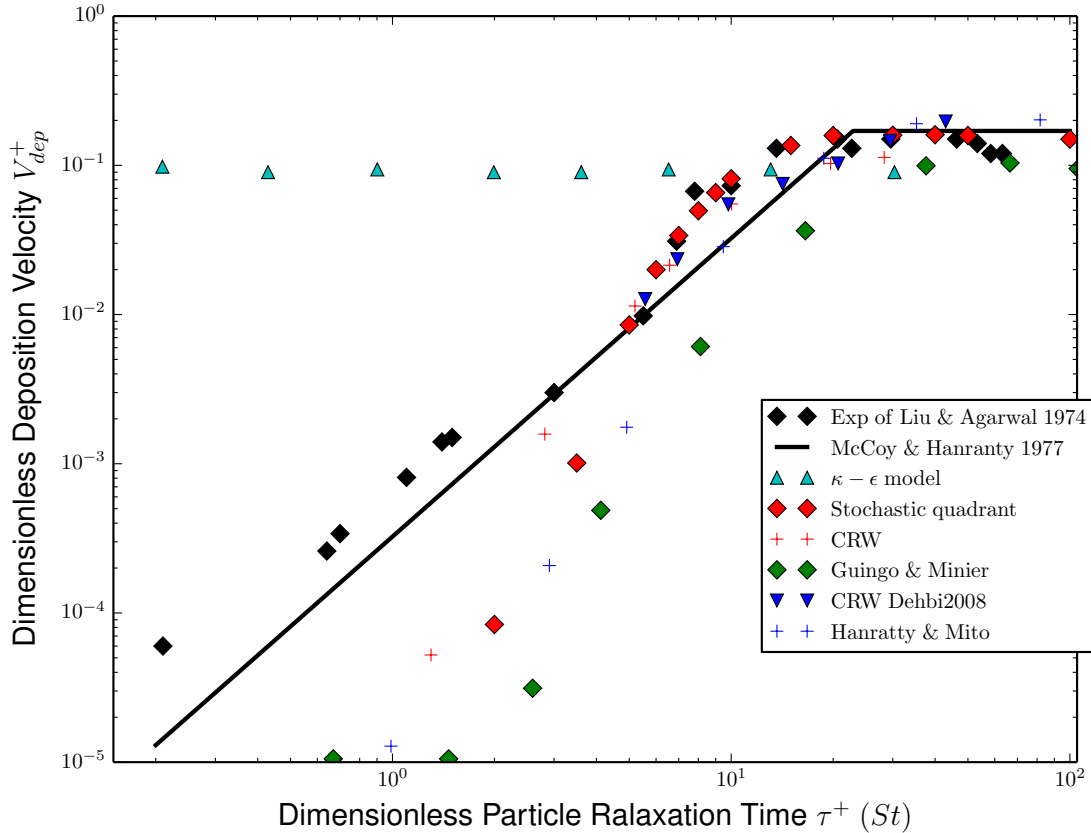


FIG. 9: Comparison of dimensionless particle deposition velocity as a function of dimensionless particle response time with experimental measurements and different models in turbulent boundary layers.

In this work, an alternative continuous random walk (CRW) model is used to repeat

the numerical study of particle deposition rates. This model is based on the wall-normal component of normalized Langevin equations in boundary layers (see^{20,46}), which takes into account the effect of Stokes number along heavy particle paths (see⁴⁷). The Langevin equation is solved using a second-order accuracy Milshstein scheme (see⁴⁸). The non-dimensional fluctuating fluid velocity solved this way was converted to a physical velocity and then added into the particle equation of motion to account for the turbulence effect.

Results for the deposition rates from this CRW model are also shown in FIG. 9. There are a few interesting points to note. Firstly, very similar results are obtained by us from this one-dimensional CRW model compared to those obtained using CRW by Dehbi²⁰. Secondly, the numerical results from all the models show fair agreement with experiments for large particles. However, they all give significant under-predictions on deposition rates for small particles. In contrast to the present one-dimensional CRW and stochastic quadrant model, the CRW model employed by Dehbi²⁰ was solved in three dimensions with curve-fitting DNS database. This may further corroborate the view that the wall-normal fluid fluctuations are a critical control factor on the deposition of heavy particles from fully developed turbulent boundary layer. Thus, as far as practical applications are concerned, it is possible and feasible to feed in only the wall-normal fluid fluctuations for studying particle deposition. On the other hand, compared to CRW models, the stochastic quadrant model is capable of yielding equally reliable results for deposition rates, given its relatively simple nature and the way it takes account of the influence of sweeps and ejections in turbulent boundary layers. As a consequence, it is potentially a very promising model for studying deposition of heavy particles from turbulent flows.

Deposition rate data obtained in the previous study of Guingo and Minier²¹, using a stochastic model to account for the coherent structures, e.g. sweeps and ejections, in turbulent boundary layers, show good agreement with experimental data plot of Papavergos and Hedley⁴⁹(who plotted all the available measured data on deposition rates at the time). As the present stochastic quadrant model also accounts for such features in turbulent boundary layers, it is worth comparing our predicted deposition rates with the same experimental data as Guingo and Minier have done. FIG. 10 shows the comparison. As can be seen, the predicted deposition rates from the present stochastic model fall well into the middle realm of experimental data of Papavergos and Hedley thanks to the larger scatter of the experimental data.

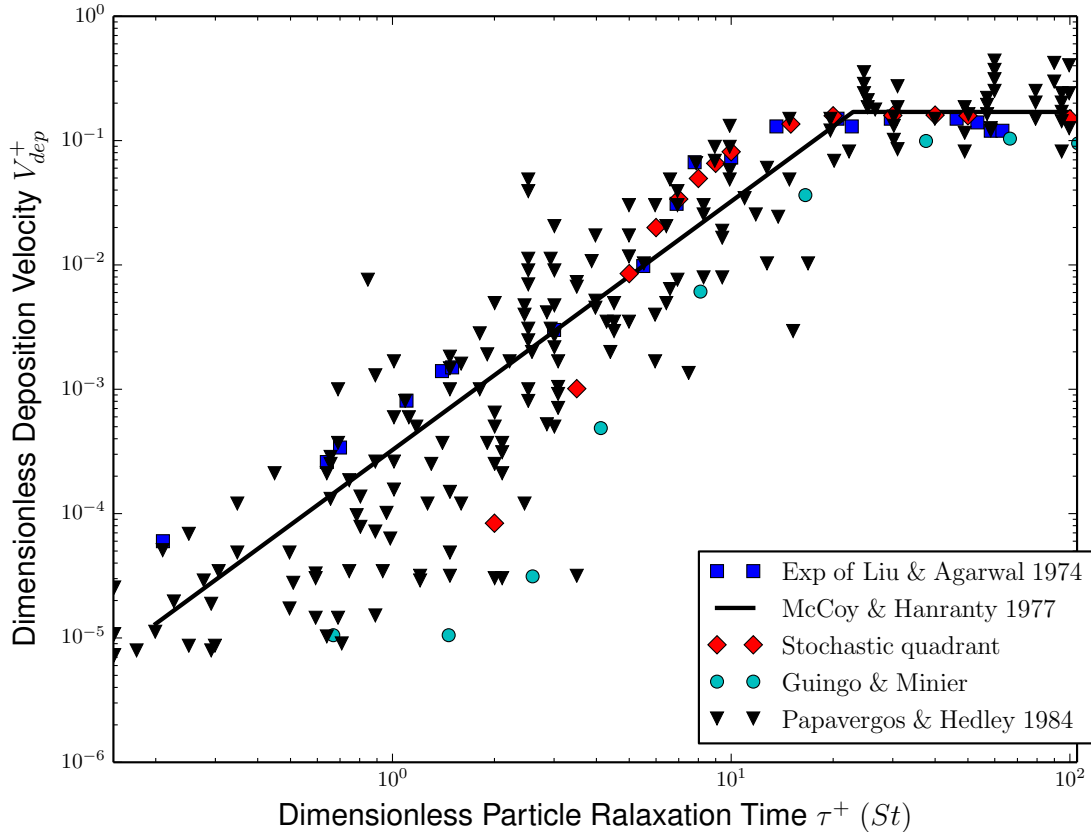


FIG. 10: Comparison of dimensionless particle deposition velocity as a function of dimensionless particle response time with experimental measurements.

2. Mean particle concentration

FIG. 11 shows the mean particle concentration profile as a function y^+ across the boundary layer assuming no inter-particle collisions. There is a significant build-up in concentration for the four classes of particles within the viscous sublayer. This build-up of particles near the wall has been observed by numerous researchers (see^{6,33,50}) and is attributed to turbophoresis in the very near wall region (see⁵¹). The gradient in wall-normal fluid fluctuations in boundary layer turbulence acts as a driving force and results in a wall-ward net flux. The build-up concentration of particle with $St = 20$ is smaller than those of smaller particles with $St = 2, 5, 10$. This may result from the fact that these particles are too inert to follow the relatively quiescent viscous sublayer. On the other hand, they may move across the viscous sublayer by free flight and deposit on the wall, which may also be responsible

for the relative reduction of build-up.

The positions of the peak concentration can be explained as a combination of turbophoretic drift and turbulent diffusion. Very close to the wall they enhance one another whilst further away they oppose one another. In either case there is a constant wall-ward flux and a peak concentration near the wall whose precise location depends upon the divergence of the particle kinetic stresses. In the 1-D model it's simply the gradient of particle mean square velocity. In comparing the concentration profiles of our model with those of the Guingo and Minier (G&M) model²¹, we note that the turbophoretic drift will be significantly different because the profile of the normal kinetic stresses in the G&M model will be steeper. This will also influence the local eddy diffusion coefficient. An important feature of this balance between drift and diffusion and its dependence on particle Stokes number, is that there will be a peaking of the particle concentration (near the wall) and that its value and location will vary with particle Stokes number. In particular there will be a maximum value which if the Stokes number is defined properly in terms of the ratio of particle relaxation time to the timescale of the local fluid motion, will occur for $St \sim 1$. Note that St in this paper and elsewhere is taken to be τ^+ , the Stokes relaxation time in wall units. The fact that this maximum peaking with St was not observed in the G&M concentration profiles, probably means that the G&M had not gone far enough in their values of St . This behaviour is consistent with important features of preferential concentration which is known to have a maximum effect for particles with Stokes numbers ~ 1 . To our knowledge, there is no universal agreement on the (y^+) position of the peak particle concentration. We refer to the DNS studies by Marchioli *et al.*⁵², from which the peak particle concentration seems to be at position $y^+ < 1$. See also the results of an international collaborative benchmark test by multiple research groups⁵² which show a similar peaking of the concentration around $y^+ \sim 1$.

This reduction in the peak concentration and a noticeable rise in the form of the concentration profiles near the edge of the boundary layer for $St = 20$ shown in FIG. 11 are also features of the concentration profiles of the PDF calculations of van Dijk and Swailes¹³, They can be explained more explicitly in terms of a competition between turbophoresis and particle diffusion and their individual dependence on the particle response time τ_p (equivalent to St when it is expressed in wall units). The particle diffusion coefficient ϵ_p and the

turbophoretic drift velocity v_T are explicitly dependent upon τ_p as

$$\epsilon_p = \epsilon_{pf} + \tau_p \langle v_p'^2 \rangle \quad v_T = -\tau_p \frac{d \langle v_p'^2 \rangle}{dy} \quad (22)$$

where $\langle v_p'^2 \rangle$ is the particle mean square velocity and ϵ_{pf} the particle-fluid diffusion coefficient in the normal streamwise direction^{8,53}. Both ϵ_p and v_T are implicitly dependent upon y the distance away from the wall and also upon particle inertia through the dependence of $\langle v_p'^2 \rangle$ and ϵ_{pf} on τ_p which is essentially *non-local* except for very small inertia particles. So the equation for the concentration $\rho(y)$ (normalised by the concentration at the edge of the boundary layer) for a constant deposition flux depends upon the ratio of $v_T L / \epsilon_p$

$$d\rho/dy = [K - |v_T(y)| \rho(y)] L / \epsilon_p(y) \quad (23)$$

where K is the deposition velocity (mass transfer coefficient) and L is the effective boundary layer thickness (~ 100 in wall units in our calculation). At the edge of the boundary layer $|v_T(y)| / K \ll 1$, so $d\rho/dy \geq 0$ and the concentration always rises as we approach the boundary layer edge. The steepness or flatness of the curve in this region will depend on the value of $KL / \epsilon_p(y)$. Both K and ϵ_p increase with τ_p . So the fact that this ratio increases with increasing τ_p , giving a steeper curve, is because K increases faster than ϵ_p / L as a function of τ_p near the boundary layer edge.

The peak ρ_{max} will occur away from the wall for depositing particles, and is given by

$$\rho_{max} = K / v_T \quad (24)$$

So although the deposition velocity K increases with increasing τ_p so does the turbophoretic velocity v_T . However the ratio K / v_T for $St = 20$, is lower than it is for the other values of $St = 2, 5, 10$.

3. Mean wall-ward drift velocity and Root mean square (rms) velocity profiles

FIGs. 12 and 13 show the mean wall-ward drift and sampled fluid velocity profiles in the near wall region. We observe that the four sets of particles, $St = 2, 5, 10, 20$, have non-zero wall-ward mean velocity (negative) values. This indicates that the present stochastic quadrant model predicts the phenomenon of turbophoresis. This wall-ward mean velocity

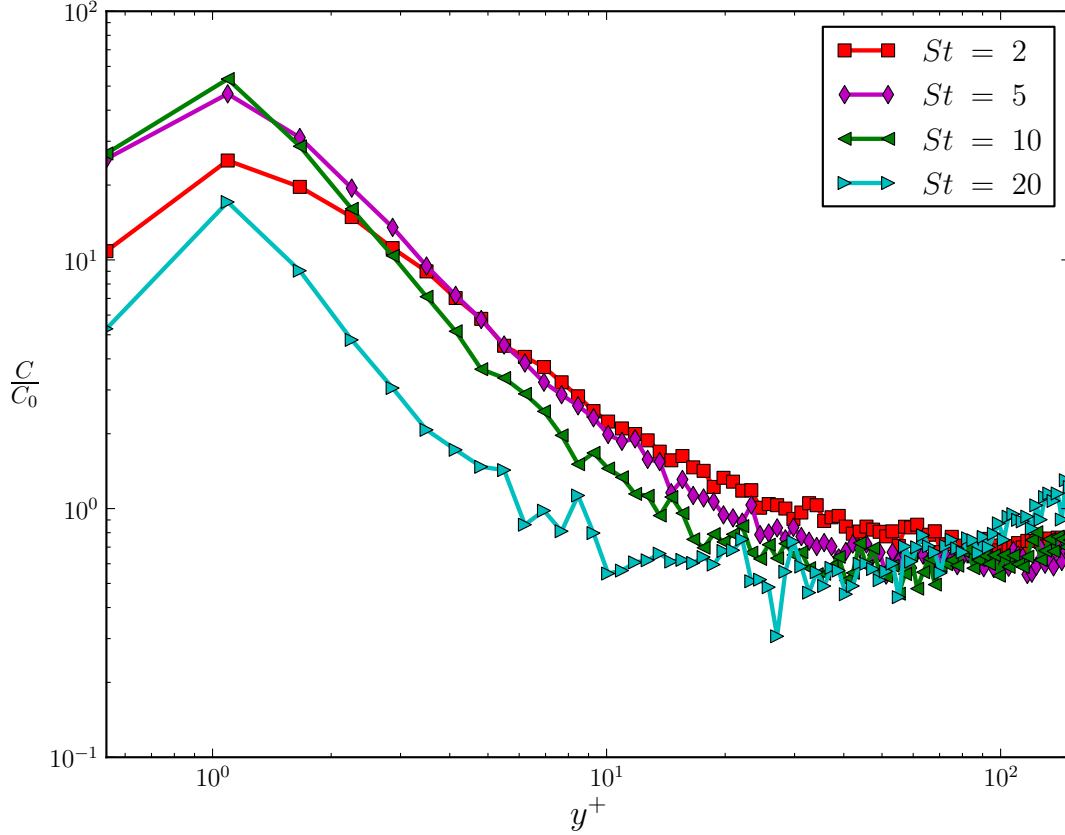


FIG. 11: Particle preferential concentration profile as a function of y^+ .

of heavy particles results primarily from the turbulence gradient of the boundary layer turbulence as well, which is the prime mechanism responsible for the build-up of particles. It is observed that the mean wall-ward drift velocity of particles varies monotonically with the increase of the particle inertia. Although the wall-normal fluid velocity has zero mean, the sampled mean fluid velocity at the particle location has positive values.

The existence of the wallward particle flux ties in with the particle concentration profile which shows peaking near the wall consistent with the existence of a turbophoretic drift towards the wall and a diffusive flux whose direction depends upon the near wall concentration gradient. It is clear that beyond the peak concentration, the concentration gradient is negative with respect to y^+ indicating that the diffusive flux is in a direction away from the wall. However the particle flux is still directed towards the wall. It indicates that there is a flux (independent of the concentration gradient) that is directed towards the wall and noticeably

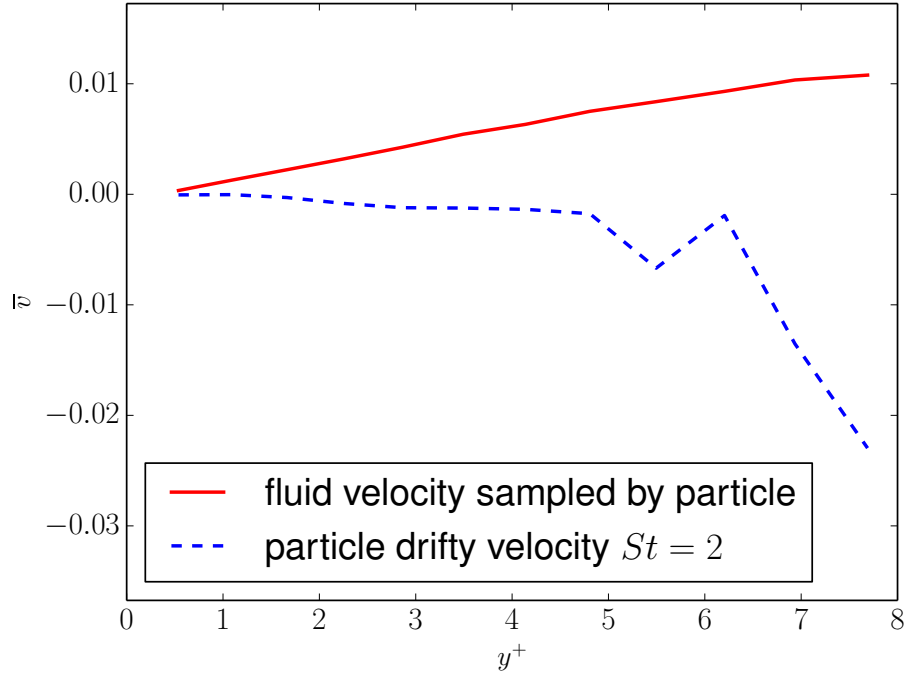
greater than the diffusive flux. This is of course the contribution due to turbophoresis.

The mean wall-ward fluid velocity \bar{v} sampled by the particles is an important quantity in two-fluid modelling and much effort has gone into its dependence on the particles' response time⁵³. Like the mean fluid velocity (sampled by a fluid element) it is generally considered to be diffusive. The values of \bar{v} plotted in FIGs. 12 and 13 are consistent with the diffusive nature, i.e., when the concentration gradient is negative beyond the peak value of the concentration, it is directed away from the wall.

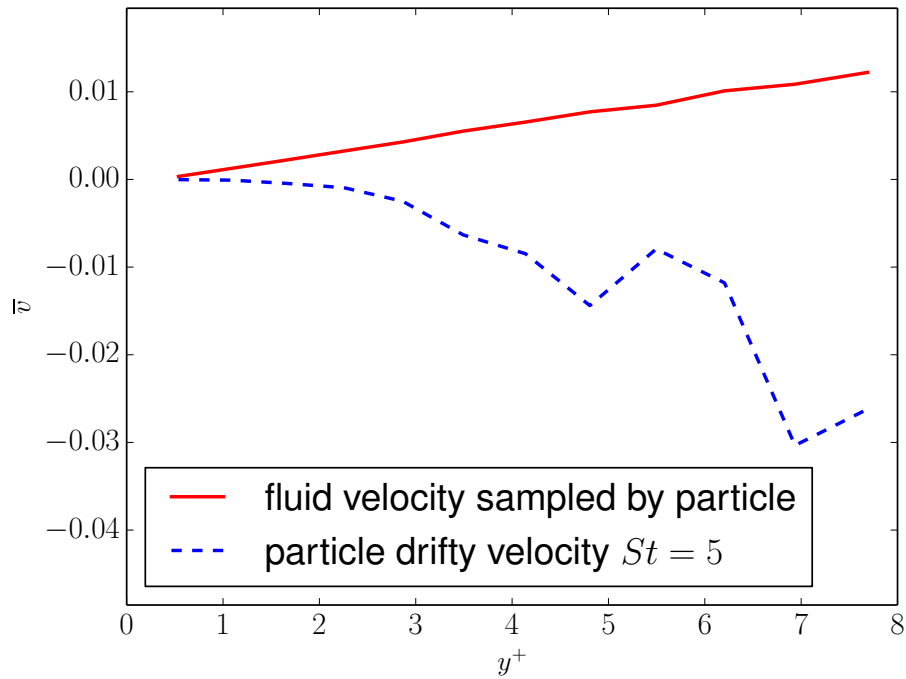
FIGs. 14 and 15 show the comparison of the rms of velocity fluctuations of four sets of particles with the fluid velocity fluctuations. It is observed that the r.m.s of particle phase is significantly different from the fluid phase. The difference increases with increasing particle inertia. This results from the fact that the heavier the particles, the slower their response to the change of surrounding fluid. As far as the raggedness displayed in the computed particle r.m.s profile is concerned, the explanation may be that the particle phase still has not reached equilibrium or that each sampling bin does not have a sufficient number of representative particles.

4. Mechanisms for particle deposition

The present stochastic model has also been used to study the mechanisms for particle deposition. By analysing extensively the DNS data-sets for particle transport in turbulent boundary layers, Brooke, Hanratty, and McLaughlin⁵⁴ and Narayanan *et al.*⁵⁰ attributed deposition to two different mechanisms depending on the particle inertia (Stokes number, St). Relatively low inertia particles deposit by a diffusion mechanism, whilst high inertia particles deposit as a result of free-flight. To differentiate between the two mechanisms, the concept of particle residence time is introduced namely the continuous time spent by a particle within a certain wall region before depositing. Particles depositing through diffusion have relatively smaller values of deposition velocity and larger values of residence time. In contrast, particles depositing via the free-flight mechanism have the opposite values, that is relatively larger values of deposition velocity and smaller values of residence time. For the deposition velocities and residence time, FIG. 16 shows a scatter plot of wall-normal deposition velocities as a function of particle residence time within the region of $y^+ < 3$. The red curve is plotted according to the relation between the wall normal deposition velocity

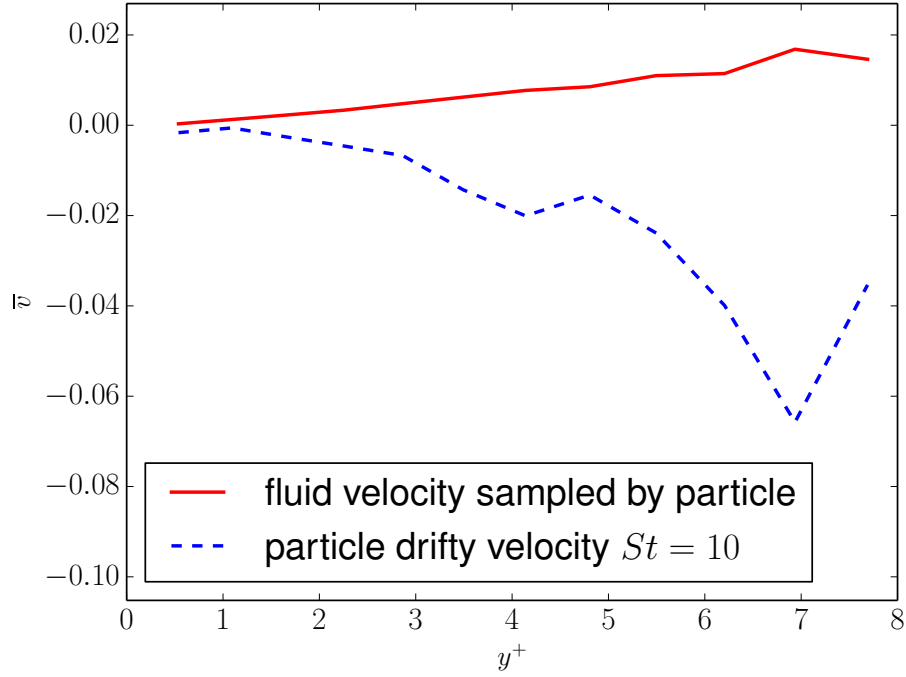


(a)

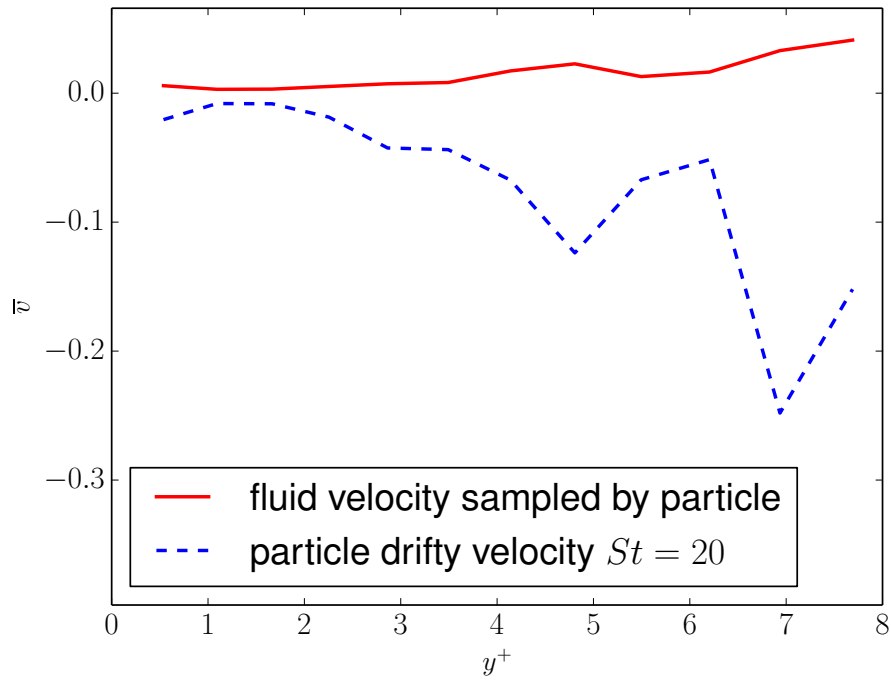


(b)

FIG. 12: Mean fluid wall-ward velocity sampled by particle and particle wall-ward drift velocity \bar{v} , (a) $St = 2$, (b) $St = 5$.

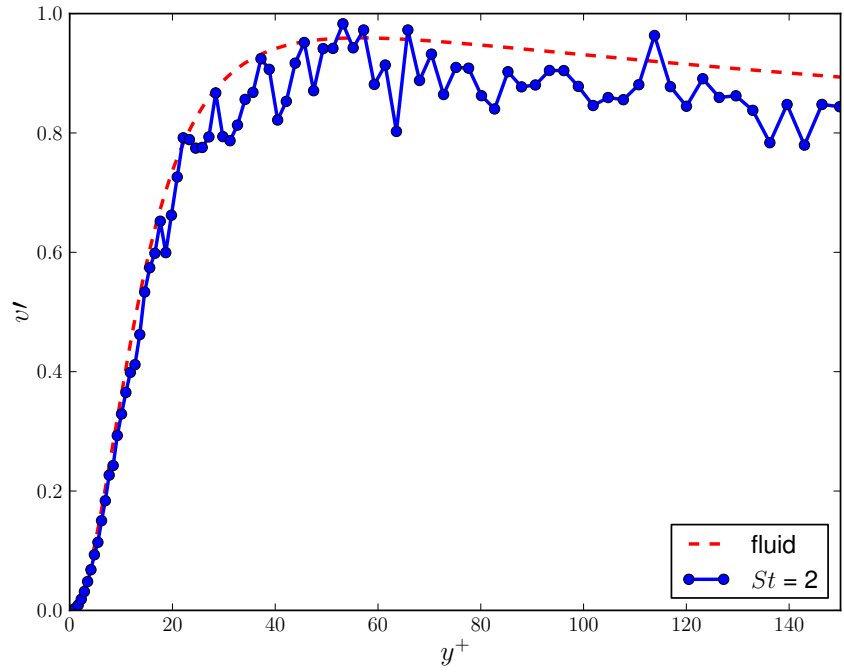


(a)

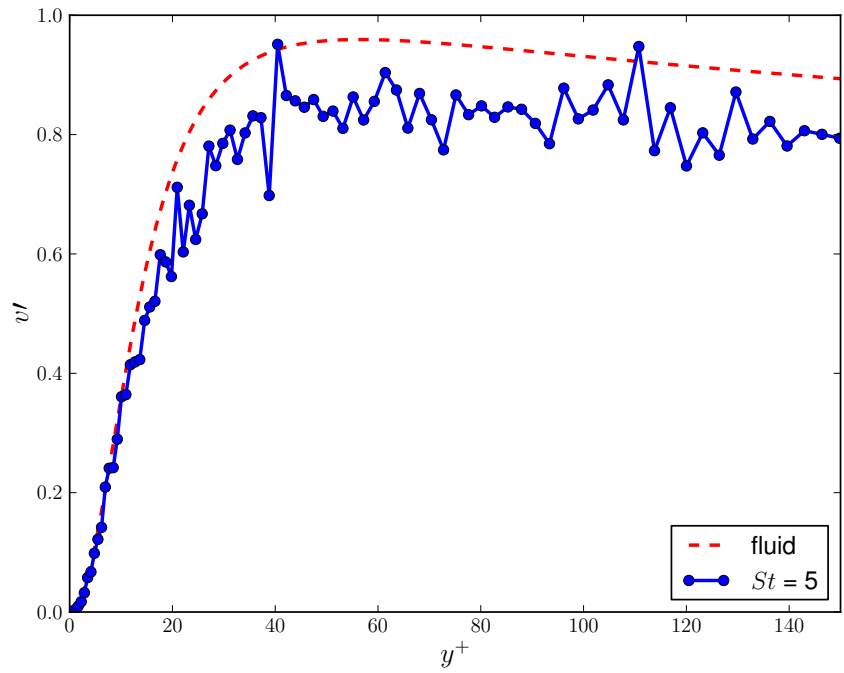


(b)

FIG. 13: Mean fluid wall-ward velocity sampled by particle and particle wall-ward drift velocity \bar{v} , (a) $St = 10$, (b) $St = 20$.

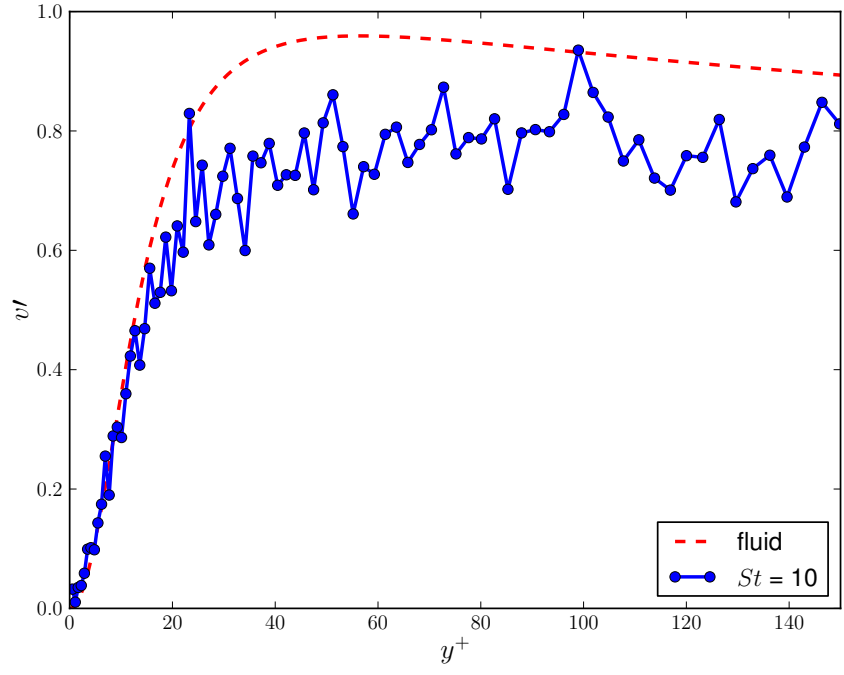


(a)

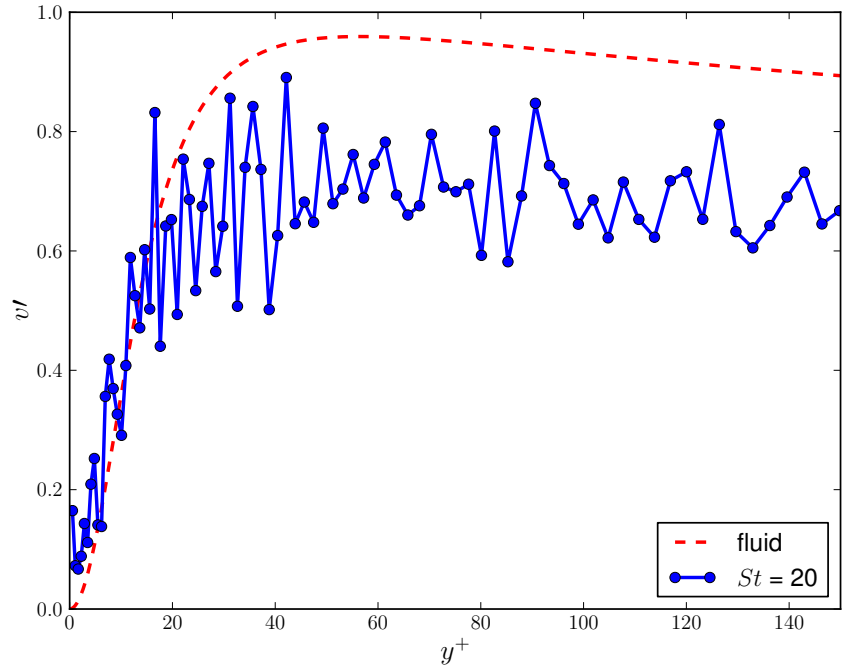


(b)

FIG. 14: Root mean square (r.m.s) of velocity fluctuations, (a) $St = 2$, (b) $St = 5$.



(a)



(b)

FIG. 15: Root mean square (r.m.s) of velocity fluctuations, (a) $St = 10$, (b) $St = 20$.

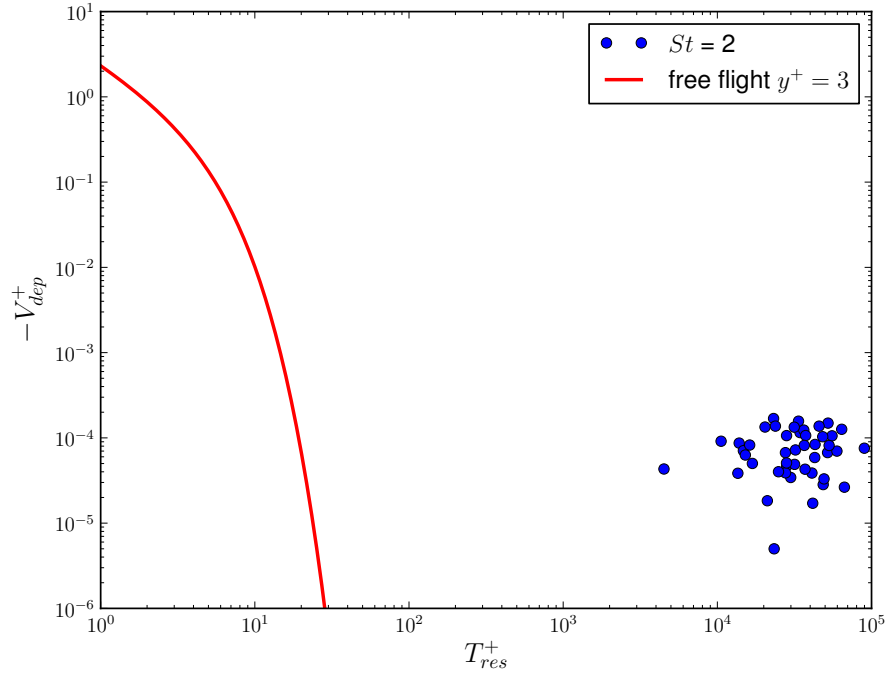
V_{dep}^+ and the residence time T_{res}^+ provided by Narayanan *et al.*⁵⁰

$$V_{dep}^+ = \frac{3 - d_p^+/2}{\tau^+ \left[1 - \exp\left(\frac{T_{res}^+}{\tau^+}\right) \right]}, \quad (25)$$

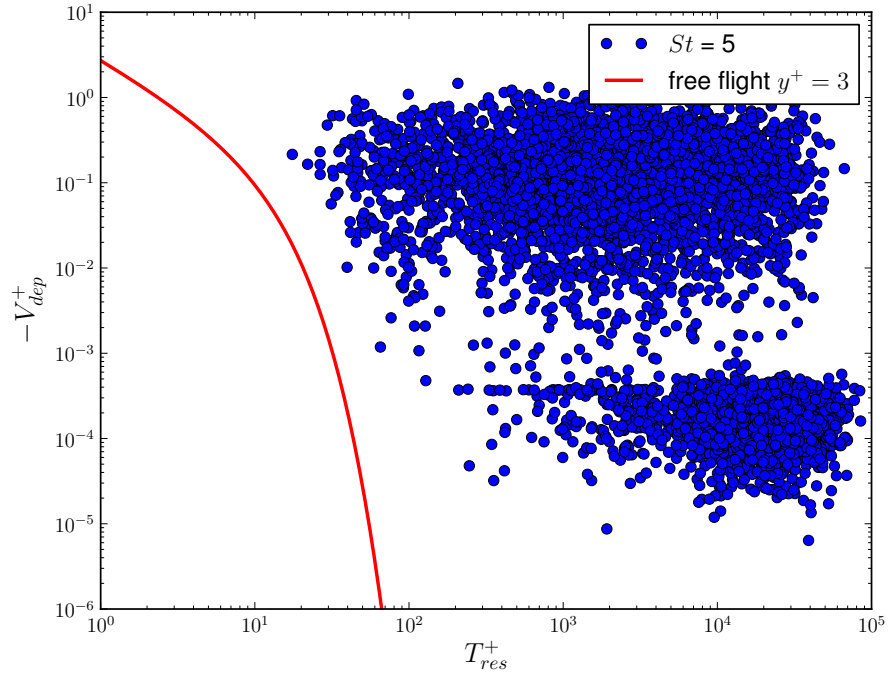
where d_p is the non-dimensional particle diameter based on the free-flight theory³. It can be observed that the deposited particles with $St = 2$ do not follow the free flight theory defined by Eq: 25 as they assume relatively large near-wall residence time and a small deposition velocity. These particles are usually referred to as the diffusion deposition population⁵⁰. For the particles with $St = 5$, there are two distinct populations of particles. The first population assumes very long near-wall residence time and negligible deposition velocity; however, the second population still assumes a relatively long near-wall residence time but relatively large deposition velocities. The first population of particles, may be identified as diffusion deposition particles. The near-wall residence time for the second population is different from the DNS data calculated by Narayanan *et al.*⁵⁰ as they do not follow the free flight curve defined in Eq: 25. But the magnitude of deposition velocity of this population particles falls into the correct range of $[10^0, 10^{-3}]$ as shown by Narayanan *et al.*⁵⁰. For all the deposited particles, the majority falls into the second population and does not conform to the free flight particles residence times as one might have expected. We take that to suggest a possible alternative mechanism. As far as the over-prediction of near-wall residence time compared to the DNS data is concerned, these particles may experience significant repeated events both in quadrant IV (sweeps) and in quadrant II (ejections) within the viscous sublayer, and the events in quadrant II cause particles to be re-entrained to the outer layer or to coast along the wall surface within the region of $y^+ < 3$ with relatively larger velocities before being deposited. As a consequence, they assume relatively larger velocities and larger near-wall residence time at the same time. However it is clear that this behaviour requires further investigation along with our proposed mechanism arising from ejection and sweeping events.

5. A note on the influence of segregation on deposition

This is reflected in the contribution segregation has on the net drift velocity of particles towards the wall and it is the combination of drift versus diffusion away from the wall that leads to a build-up of particle concentration near the wall. The drift velocity is referred to as turbophoresis because when it was first invoked it referred to the migration of particles in an



(a)



(b)

FIG. 16: Particle residence time in the region of $y^+ < 3$ versus particle deposition velocity

(a) $St = 2$, (b) $St = 5$.

inhomogeneous turbulent flow from regions of high to low regions of turbulence intensity⁵¹. More precisely the turbophoretic velocity is given by

$$v_{T,i} = -\tau_p \frac{\partial \langle v'_{p,j} v'_{p,i} \rangle}{\partial x_j} \quad (26)$$

where $\langle v'_{p,j} v'_{p,i} \rangle$ are the particle kinetic stresses per unit mass and τ_p is the particle relaxation or response time. The formula reflects a balance between the drag and the gradients of the particle kinetic stress at equilibrium. In the case of a fully developed boundary layer, the drift velocity towards the wall simply reduces to $v_T = -\tau_p d \langle v_p'^2 \rangle / dy$. It has nothing to do directly with the persistence or scale of the turbulent structures in the flow that is the direct cause of segregation.

The influence of segregation (un-mixing) has been shown to manifest itself as an extra drift that depends upon the compressibility of the particle velocity flow field along a particle trajectory⁵³: Reeks has referred to it as Maxey drift because it is the same expression for the enhancement of settling under gravity due to turbulent structures in a homogeneous turbulent flow⁵⁵. For a flow field generated by a Langevin equation involving a white noise driving force, the drift is zero because the flow field generated has no structure to it (it has zero spatial correlation). The turbulent flow field generated in this simulation does give rise to an extra drift other than that due to turbophoresis⁵¹ because it has persistence both in space and time and is spatially inhomogeneous. However it is likely that in real boundary layer flows the combination of vorticity and straining would lead to more pronounced segregation, a greater enhanced drift and to greater deposition rates than predicted by current stochastic CRW models.

6. Probability density function (pdf) of impact velocities of particles

FIGs. 17 and 18 show the PDF of non-dimensional wall-normal impact velocities of depositing particles at the wall. We see that there is a large increase in probability in the first bin for the three sets of particles. The particles falling in this bin may be associated with the population of particles depositing by diffusion. There also exists a long trail of high impact velocities, indicating some of the depositing particles have high deposition velocities. They may be associated with free-flight particles. The PDF of $St = 20$ is much wider than those of $St = 5, 10$, indicating that heavier particles are transported by free-flight across the

viscous sublayer before deposition¹³.

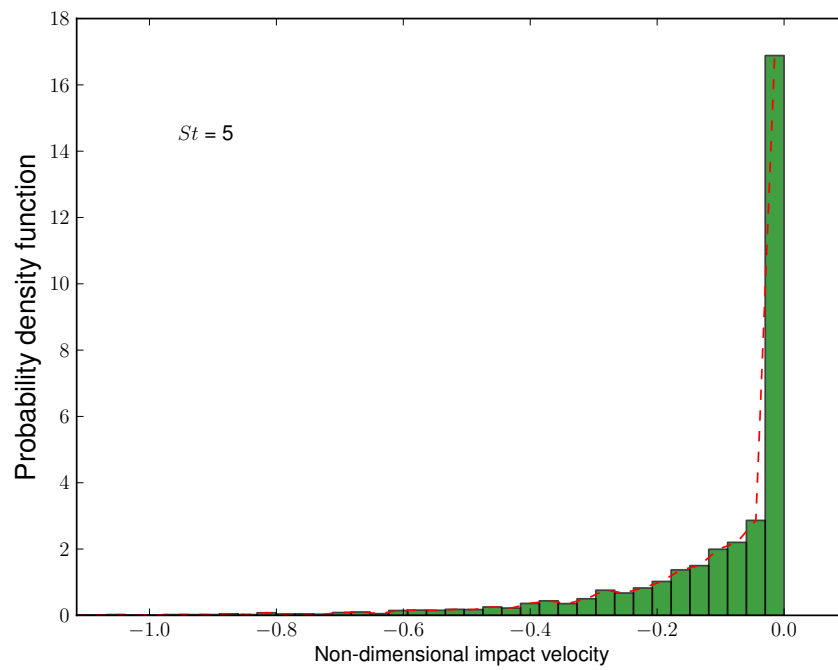
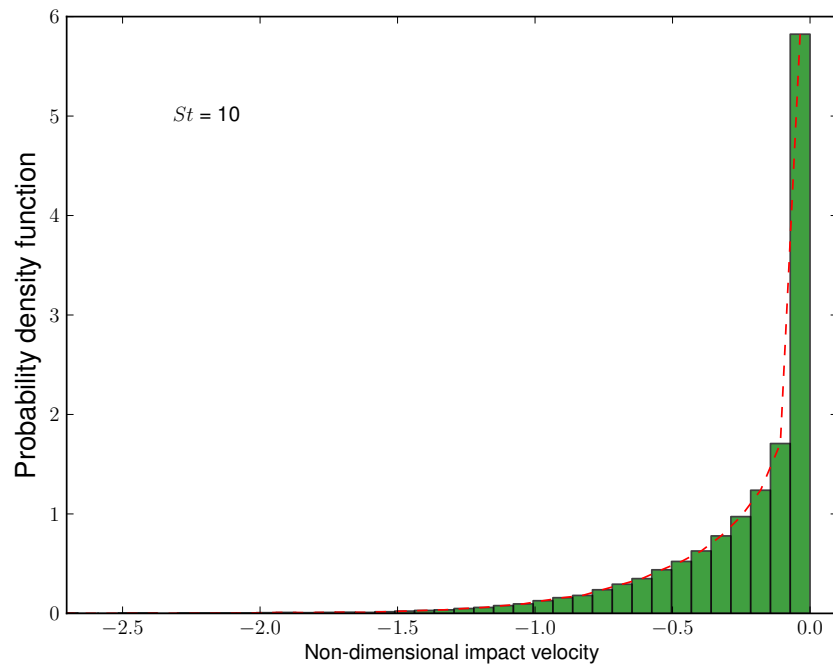
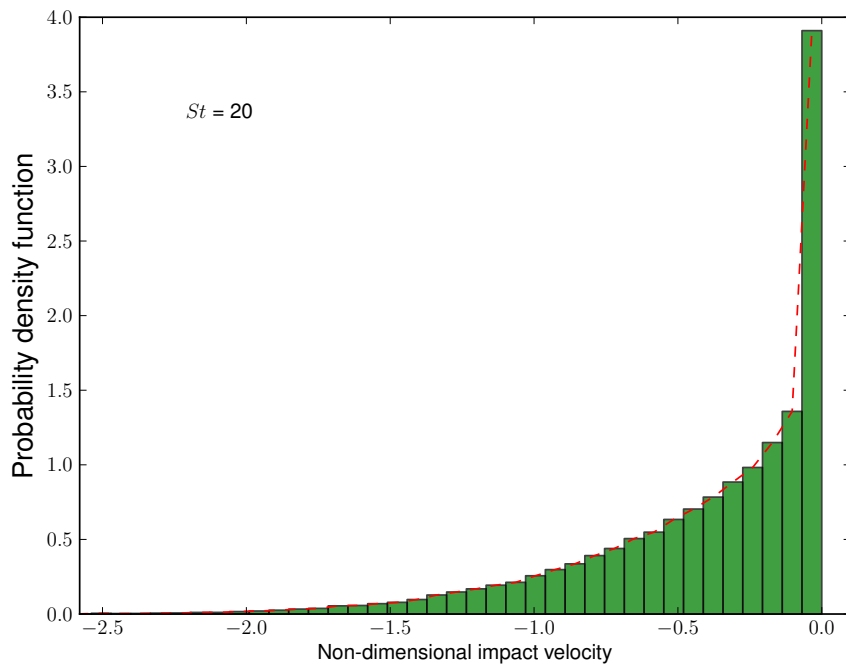


FIG. 17: Probability density function (pdf) of non-dimensional impact velocities of particles, $St = 5$.



(a)



(b)

FIG. 18: Probability density function (pdf) of non-dimensional impact velocities of particles, (a) $St = 10$, (b) $St = 20$.

IV. CONCLUDING REMARKS

We have described a novel stochastic quadrant model for investigating the transport and deposition of heavy particles in a fully developed turbulent boundary layer inspired by the quadrant analysis of the Reynolds stress domain by Willmarth and Lu¹. The detailed statistics of each quadrant are based on a quadrant analysis of the wall-normal fluid velocity fluctuations obtained by an LES of a fully developed channel flow. The turbulent dispersion of heavy particles in a fully developed turbulent boundary layer is modeled as interactions of heavy particles with a succession of random eddies generated in four quadrants via a homogeneous Markov chain process and was naturally consistent with the skewness of wall-normal fluid velocity fluctuations observed in fully turbulent developed boundary layers. In so doing the model captures the influence of sweeps and ejections in the near wall region of the boundary layer on the particle deposition process. This model yields very good predictions of the deposition rate for particles with $St > 5$ when compared with benchmark experimental measurements. Prediction of deposition rates at lower values of St gives a significant underestimation and may need further improvement. In addition, the deposition rates obtained by the stochastic quadrant model was compared with that acquired by solving a one-dimensional Langevin equation based on a continuous random walk (CRW) model as well as results from other CRW models. The discrepancy between deposition rates for particles with $St > 5$ is minor. When compared to the stochastic ejection and sweep deposition model of Guingo & Miner²¹, an important feature of the present model is its simplicity and transparency without the need for ad-hoc tuning of model parameters. The present data are statistically consistent with experimental analysis of coherent structures in a turbulent boundary layer and is much simpler to implement in RANS CFD modelling frameworks than the model of Guingo and Minier²¹.

Most of the predicted statistics of heavy particles are consistent with experimental measurements and DNS calculations. Build-up of particle concentration is observed in the near wall region. This indicates that the present stochastic model is capable of predicting turbophoresis regarded as responsible for this build-up. The related mean wallward drift velocity is predicted in the viscous sublayer. Predicted profiles of heavy particles wall-normal r.m.s. velocity are typically lower than the counterpart of fluid particles. Mechanisms for particle deposition are explored by observing particle residence time versus deposition veloc-

ity. Clearly as indicated by the residence time versus deposition velocity shown in FIG. 16 in the case for $St = 2$, particles reach the wall by turbophoresis/diffusion. There are no free flight particles. The case for FIG. 16b is most interesting because although the particles separate into two distinct populations, the regime of particles associated with the significantly higher deposition velocities do not conform to the free flight particles residence times as one might have expected. We have taken that to suggest a possible alternative mechanism. However it is clear that this behaviour requires further investigation along with our proposed mechanism arising from ejection and sweeping events. Studying the behaviour of higher inertial particles in the regime where there is good agreement with experiment would be useful in establishing when a free flight mechanism make a contribution.

The major drawbacks in the present stochastic models lie in the Lagrangian integral time scales for the random eddies occurred in four quadrants and in the inherent spurious drift associated with discrete random walk models. The latter disadvantages may be corrected by introducing an appropriate component into the particle equation of motion for the wall-normal fluid velocity fluctuation (see⁵⁶). However, the time scales for the events in the four quadrants still call for further investigations.

Finally it is important to recall the concerns we expressed about the applicability of using this approach to calculate particle deposition in more complex flows other than in the fully developed turbulent channel flow which has been the focus of the study we have presented here. As with other stochastic models we imply its application in conjunction with a RANS calculation of the underlying flow e.g $k - \epsilon$. So in complex flows, such as over cylinders or tube-banks where the shear stress varies rapidly around the wall surface, the model developed in this work as with other stochastic models share the inherent wall shear stress approximations of a RANS model employing wall functions, which may lead to significant local errors. It is in these sorts of flows that more detailed LES calculations of the sort carried out for turbulent channel the LES are required.

In using LES in this way, a natural and legitimate question to ask is “why use a stochastic model when one can use LES directly”. The reason is one of computational efficiency or perhaps more precisely a matter of reliability and statistical accuracy. There is a lot of statistical information contained in an LES calculation which is not wholly relevant when we use it to calculate particle deposition. So the construction and application of a simple stochastic model of the sort described and studied in this paper has been to extract the

most relevant and most appropriate information about near wall turbulent flow that is important in accurately predicting deposition and to incorporate this into a model in the most computationally efficient way. Such a model can then be used to calculate particle deposition for a whole range of particles sizes, flows and particle wall boundary conditions (from perfectly absorbing to partially absorbing).

ACKNOWLEDGMENTS

The financial support and advice of British Energy (part of EDF Energy, Barnwood, Gloucester, U.K.) is gratefully acknowledged. However the views expressed in this paper are those of the authors and do not necessarily represent the views of the sponsors. The authors would also like to thank Dr. David C. Swailes for the insightful discussions on the development of the stochastic quadrant model. Finally, we wish to acknowledge the anonymous reviewers for useful feedback on the revision of this paper.

REFERENCES

- ¹W. W. Willmarth and S. S. Lu, “Structure of the reynolds stress near the wall,” *Journal of Fluid Mechanics* **55**, 65–92 (1972).
- ²S. K. Friedlander, *Smoke, Dust, and Haze: Fundamentals of Aerosol Dynamics*, 59New York: *Oxford University Press* (2000).
- ³S. K. Friedlander and H. F. Johnstone, “Deposition of suspended particles from turbulent gas streams,” *Industrial & Engineering Chemistry* **49**, 1151–1156 (1957).
- ⁴C. N. Davies, “Deposition of aerosols from turbulent flow through pipes,” *Proceedings of the Royal Society of London. Series A, Mathematical and Physical Sciences* (1934-1990) **289**, 235–246 (1966).
- ⁵P. Hutchinson, G. F. Hewitt, and A. E. Dukler, “Deposition of liquid or solid dispersions from turbulent gas streams: a stochastic model,” *Chemical Engineering Science* **26**, 419–439 (1971).
- ⁶G. A. Kallio and M. W. Reeks, “A numerical simulation of particle deposition in turbulent boundary layers,” *International Journal of Multiphase Flow* **15**, 433–446 (1989).
- ⁷D. C. Swales and M. W. Reeks, “Particle deposition from a turbulent flow. i. a steady-state model for high inertia particles,” *Physics of Fluids* **6**, 3392 (1994).
- ⁸M. W. Reeks, “On a kinetic equation for the transport of particles in turbulent flows,” *Physics of Fluids A: Fluid Dynamics* **3**, 446 (1991).
- ⁹J. Young and A. Leeming, “A theory of particle deposition in turbulent pipe flow,” *Journal of Fluid Mechanics* **340**, 129–159 (1997).
- ¹⁰A. Guha, “A unified eulerian theory of turbulent deposition to smooth and rough surfaces,” *Journal of Aerosol Science* **28**, 1517–1537 (1997).
- ¹¹L. I. Zaichik, N. I. Drobyshvsky, A. S. Filippov, R. V. Mukin, and V. F. Strizhov, “A diffusion-inertia model for predicting dispersion and deposition of low-inertia particles in turbulent flows,” *International Journal of Heat and Mass Transfer* **53**, 154–162 (2010).
- ¹²P. Nerisson, O. Simonin, L. Ricciardi, A. Douce, and J. Fazileabasse, “Improved cfd transport and boundary conditions models for low-inertia particles,” *Computers & Fluids* **40**, 79–91 (2011).
- ¹³P. van Dijk and D. Swales, “Hermite-dg methods for pdf equations modelling particle transport and deposition in turbulent boundary layers,” *Journal of Computational Physics*

- 231**, 4904 – 4920 (2012).
- ¹⁴C. Greenfield, *Numerical modelling of transport phenomena in reactors*, Ph.D. thesis, Bristol Univesity (1998).
- ¹⁵E. A. Matida, K. Nishino, and K. Torii, “Statistical simulation of particle deposition on the wall from turbulent dispersed pipe flow,” *International Journal of Heat and Fluid Flow* **21**, 389–402 (2000).
- ¹⁶C. Kroer and Y. Drossinos, “A random-walk simulation of thermophoretic particle deposition in a turbulent boundary layer,” *International Journal of Multiphase Flow* **26**, 1325–1350 (2000).
- ¹⁷L. Tian and G. Ahmadi, “Particle deposition in turbulent duct flows - comparisons of different model predictions,” *Journal of Aerosol Science* **38**, 377–397 (2007).
- ¹⁸A. Dehbi, “A CFD model for particle dispersion in turbulent boundary layer flows,” *Nuclear Engineering and Design* **238**, 707–715 (2008).
- ¹⁹M. Horn and H. J. Schmid, “A comprehensive approach in modeling lagrangian particle deposition in turbulent boundary layers,” *Powder Technology* **186**, 189–198 (2008).
- ²⁰A. Dehbi, “Turbulent particle dispersion in arbitrary wall-bounded geometries: A coupled CFD-Langevin-equation based approach,” *International Journal of Multiphase Flow* **34**, 819–828 (2008).
- ²¹M. Guingo and J.-P. Minier, “A stochastic model of coherent structures for particle deposition in turbulent flows,” *Physics of Fluids* **20**, 053303 (2008).
- ²²S. Chibbaro and J. P. Minier, “Langevin PDF simulation of particle deposition in a turbulent pipe flow,” *Journal of Aerosol Science* **39**, 555–571 (2008).
- ²³A. Mehel, A. Tanière, B. Oesterlé, and J. R. Fontaine, “The influence of an anisotropic langevin dispersion model on the prediction of micro-and nanoparticle deposition in wall-bounded turbulent flows,” *Journal of Aerosol Science* **41**, 729–744 (2010).
- ²⁴B. Y. H. Liu and J. K. Agarwal, “Experimental observation of aerosol deposition in turbulent flow,” *Journal of Aerosol Science* **5**, 145–148, IN1–IN2, 149–155 (1974).
- ²⁵S. J. Kline, W. C. Reynolds, F. A. Schraub, and P. W. Runstadler, “The structure of turbulent boundary layers,” *Journal of Fluid Mechanics* **30**, 741–773 (1967).
- ²⁶P. R. Owen, “Pneumatic transport,” *Journal of Fluid Mechanics* **39**, 407–432 (1969).
- ²⁷J. W. Cleaver and B. Yates, “A sub layer model for the deposition of particles from a turbulent flow,” *Chemical Engineering Science* **30**, 983–992 (1975).

- ²⁸M. Fichman, C. Gutfinger, and D. Pnueli, “A model for turbulent deposition of aerosols,” *Journal of Aerosol Science* **19**, 123–136 (1988).
- ²⁹F. G. Fan and G. Ahmadi, “A sublayer model for turbulent deposition of particles in vertical ducts with smooth and rough surfaces,” *Journal of Aerosol Science* **24**, 45–64 (1993).
- ³⁰T. Wei and W. W. Willmarth, “Examination of v-velocity fluctuations in a turbulent channel flow in the context of sediment transport,” *Journal of Fluid Mechanics* **223**, 241–252 (1991).
- ³¹D. Kaftori, G. Hetsroni, and S. Banerjee, “Particle behavior in the turbulent boundary layer. i. motion, deposition, and entrainment,” *Physics of Fluids* **7**, 1095 (1995).
- ³²D. Kaftori, G. Hetsroni, and S. Banerjee, “Particle behavior in the turbulent boundary layer. ii. velocity and distribution profiles,” *Physics of Fluids* **7**, 1107 (1995).
- ³³C. Marchioli and A. Soldati, “Mechanisms for particle transfer and segregation in a turbulent boundary layer,” *Journal of Fluid Mechanics* **468**, 283–315 (2002).
- ³⁴A. Soldati and C. Marchioli, “Physics and modelling of turbulent particle deposition and entrainment: Review of a systematic study,” *International Journal of Multiphase Flow* **35**, 827–839 (2009).
- ³⁵M. R. Maxey and J. J. Riley, “Equation of motion for a small rigid sphere in a nonuniform flow,” *Physics of Fluids* **26**, 883 (1983).
- ³⁶C. Marchioli, M. Picciotto, and A. Soldati, “Particle dispersion and wall-dependent turbulent flow scales: Implications for local equilibrium models,” *Journal of Turbulence* **7**, 1–12 (2006).
- ³⁷S. A. Morsi and A. J. Alexander, “An investigation of particle trajectories in two-phase flow systems,” *Journal of Fluid Mechanics* **55**, 193–208 (1972).
- ³⁸A state-of-art composite correlation for drag coefficient and lift coefficient has been investigated and is the subject of a subsequent paper.
- ³⁹D. C. Wilcox, *Turbulence Modeling for CFD* (DCW Industries Inc., La Cañada, CA, 1993).
- ⁴⁰S. B. Pope, *Turbulent Flows* (Cambridge University Press, 2000).
- ⁴¹J. Kim, P. Moin, and R. Moser, “Turbulence statistics in fully developed channel flow at low reynolds number,” *Journal of Fluid Mechanics* **177**, 133–166 (1987).
- ⁴²M. Germano, U. Piomelli, P. Moin, and W. H. Cabot, “A dynamic subgrid-scale eddy viscosity model,” *Physics of Fluids A: Fluid Dynamics* **3**, 1760 (1991).

- ⁴³J. Kim and P. Moin, “Application of a fractional-step method to incompressible navier-stokes equations,” *Journal of computational physics* **59**, 308–323 (1985).
- ⁴⁴T. S. Luchik and T. W. G. Tiederman, “Timescale and structure of ejections and bursts in turbulent channel flows,” *Journal of Fluid Mechanics* **174**, 529–552 (1987).
- ⁴⁵D. D. McCoy and T. J. Hanratty, “Rate of deposition of droplets in annular two-phase flow,” *International Journal of Multiphase Flow* **3**, 319–331 (1977).
- ⁴⁶Y. Mito and T. J. Hanratty, “Use of a modified langevin equation to describe turbulent dispersion of fluid particles in a channel flow,” *Flow, turbulence and combustion* **68**, 1–26 (2002).
- ⁴⁷T. L. Bocksell and E. Loth, “Stochastic modeling of particle diffusion in a turbulent boundary layer,” *International Journal of Multiphase Flow* **32**, 1234–1253 (2006).
- ⁴⁸G. Mil’shtein, “A method of second-order accuracy integration of stochastic differential equations,” *Theory of Probability & Its Applications* **23**, 396–401 (1979).
- ⁴⁹P. G. Papavergos and A. B. Hedley, “Particle deposition behaviour from turbulent flows,” *Chemical Engineering Research and Design* **62**, 275–95 (1984).
- ⁵⁰C. Narayanan, D. Lakehal, L. Botto, and A. Soldati, “Mechanisms of particle deposition in a fully developed turbulent open channel flow,” *Physics of Fluids* **15**, 763–775 (2003).
- ⁵¹M. W. Reeks, “The transport of discrete particles in inhomogeneous turbulence,” *Journal of Aerosol Science* **14**, 729–739 (1983).
- ⁵²C. Marchioli, A. Soldati, J. G. M. Kuerten, B. Arcen, A. Tanière, G. Goldensoph, K. D. Squires, M. F. Cargnelutti, and L. M. Portela, “Statistics of particle dispersion in direct numerical simulations of wall-bounded turbulence: Results of an international collaborative benchmark test,” *International Journal of Multiphase Flow* **34**, 879–893 (2008).
- ⁵³M. W. Reeks, “On model equations for particle dispersion in inhomogeneous turbulence,” *International Journal of Multiphase Flow* **31**, 93–114 (2005).
- ⁵⁴J. W. Brooke, T. J. Hanratty, and J. B. McLaughlin, “Free-flight mixing and deposition of aerosols,” *Physics of Fluids* **6**, 3404 (1994).
- ⁵⁵M. R. Maxey, “Gravitational settling of aerosol particles in homogeneous turbulence and random flow fields,” *Journal of Fluid Mechanics* **174**, 441 (1987).
- ⁵⁶J. M. MacInnes and F. V. Bracco, “Stochastic particle dispersion modeling and the tracer-particle limit,” *Physics of Fluids A: Fluid Dynamics* **4**, 2809 (1992).